

## STATISTICS OF COSMOLOGICAL BLACK HOLE JET SOURCES: BLAZAR PREDICTIONS FOR GLAST

CHARLES D. DERMER<sup>1</sup>  
*Draft version June 27, 2021*

### ABSTRACT

A study of the statistics of cosmological black-hole jet sources is applied to EGRET blazar data, and predictions are made for GLAST. Black-hole jet sources are modeled as collimated relativistic plasma outflows with radiation beamed along the jet axis due to strong Doppler boosting. The comoving rate density of blazar flares is assumed to follow a blazar formation rate (BFR), modeled by analytic functions based on astronomical observations and fits to EGRET data. The redshift and size distributions of gamma-ray blazars observed with EGRET, separated into BL Lac object (BL) and flat spectrum radio quasar (FSRQ) distributions, are fit with monoparametric functions for the distributions of the jet Lorentz factor  $\Gamma$ , comoving directional power  $l'_e$ , and spectral slope. A BFR factor  $\approx 10\times$  greater at  $z \gtrsim 1$  than at present is found to fit the FSRQ data. A smaller comoving rate density and greater luminosity of BL flares at early times compared to the present epoch fits the BL data. Based on the EGRET observations,  $\approx 1000$  blazars consisting of  $\approx 800$  FSRQs and FR2 radio galaxies and  $\approx 200$  BL Lacs and FR1 radio galaxies will be detected with GLAST during the first year of the mission. Additional AGN classes, such as hard-spectrum BL Lacs that were mostly missed with EGRET, could add more GLAST sources. The FSRQ and BL contributions to the EGRET  $\gamma$ -ray background at 1 GeV are estimated at the level of  $\approx 10 - 15\%$  and  $\approx 2\% - 4\%$ , respectively. EGRET and GLAST sensitivities to blazar flares are considered in the optimal case, and a GLAST analysis method for blazar detection is outlined.

*Subject headings:* AGNs: blazars—black holes—gamma-ray bursts

### 1. INTRODUCTION

Population studies of black-hole jet sources, which include blazars, gamma-ray bursts, and microquasars, are difficult because of the unknown emission processes and beaming patterns of the relativistic jets. Moreover, the density and luminosity evolution of black-hole jet sources through cosmic time is uncertain. Here we develop a method to treat the statistics of black-hole jet sources using the  $\gamma$ -ray data alone. Although the focus of this study is radio galaxies and blazars, the method can also be applied to GRBs (Le & Dermer 2006).

The interest in population statistics of blazar sources is that an accurate determination of source density evolution is needed to identify parent populations (Urry & Padovani 1995), to chart black-hole formation and growth throughout the history of the universe (Böttcher & Dermer 2002; Cavaliere & D'Elia 2002; Maraschi & Tavecchio 2003), and to assess the contribution of black-hole jet sources to the  $\gamma$ -ray background. The isotropic  $\gamma$ -ray background (Sreekumar et al. 1998) consists of an extragalactic  $\gamma$ -ray background (EGRB) and an uncertain contribution of quasi-isotropic Galactic  $\gamma$  rays produced, for example, by Compton-scattered radiations from cosmic-ray electrons (Strong et al. 2000, 2004).

Soon after the recognition of the  $\gamma$ -ray blazar class with EGRET (Fichtel et al. 1994),  $\gamma$ -ray blazar population studies were undertaken. Chiang et al. (1995) performed a  $\langle V/V_{max} \rangle$  analysis assuming no density evolution and

showed that luminosity evolution of EGRET blazars was implied by the data. With a larger data set and using radio data to ensure the sample was unbiased in regard to redshift determination, Chiang & Mukherjee (1998) again found that evolution was required. They obtained best-fit values through the maximum likelihood method that gave an AGN contribution to the EGRB at the level of  $\approx 25\%$ .

Stecker & Salamon (1996) postulated a radio/ $\gamma$ -ray connection, and tried to correct for the duty cycle and  $\gamma$ -ray spectral hardening of flaring states. They found that essentially 100% of the EGRET EGRB arises from unresolved blazars and AGNs. They did not, however, fit the blazar redshift distribution to provide a check on their model. The crucial underlying assumption of this approach, which has been developed in further detail in recent work (Giommi et al. 2006; Narumoto & Totani 2006), is that there is a close connection between the radio and  $\gamma$ -ray properties of blazars. Because a large number of EGRET blazars (FSRQs) are found in the 5 GHz,  $> 1$  Jy Kühr et al. (1981) catalog, a radio-/ $\gamma$  ray correlation is expected, but is not found in 2.7 and 5 GHz monitoring of EGRET  $\gamma$ -ray blazars (Mücke et al. 1997). X-ray selected BLs are also not well-sampled in radio surveys. Studies based on correlations between the radio and  $\gamma$ -ray emissions from blazars may therefore be based on a questionable foundation. It is therefore necessary to distinguish between the very different properties and histories of FSRQs and BLs and their separate contributions to the EGRB.

A detailed physical model to treat blazar statistics that avoids any radio/ $\gamma$ -ray blazar correlation was developed by Mücke & Pohl (2000). Blazar spectra were

<sup>1</sup> E. O. Hulburt Center for Space Research, Code 7653  
Naval Research Laboratory, Washington, D.C. 20375-5352; dermer@gamma.nrl.navy.mil

calculated assuming an injection electron number index of  $-2$ . Distributions in injected particle energy into BL and FSRQ jets were considered in the modeling. The indices in the injected energy distributions were taken from the luminosity functions of FR1 and FR2 radio galaxies which, according to the blazar unification scenario (Urry & Padovani 1995), are the parent populations of BLs and FSRQs, respectively. A simple description of density evolution is given in the form of a cutoff at some maximum redshift  $z_{max}$ . Depending on the value of  $z_{max}$ , Mücke & Pohl (2000) concluded that as much as  $\approx 40 - 80\%$  of the EGRB is produced by unresolved AGNs, with  $\approx 70 - 90\%$  of the emission from FR1s and BLs.

Here we also treat a physical model for FSRQs and BLs. This is similar to the study of Mücke & Pohl (2000), though different in a number of important ways. No detailed radiation modeling is employed, but rather we use mean spectral indices as measured by EGRET. Various model forms describe the rate density of blazar flares, but only single values of luminosity and  $\Gamma$  factor are considered for each of the FSRQ and BL classes. A mono-luminosity function for blazars means that the range in apparent powers is kinematic, arising from the different, randomly oriented jet directions. This simple blazar model is highly constrained when fitting to data, even given the freedom to consider different redshift-dependent analytic forms for the blazar formation rate (BFR). In the case of detailed fits to blazar data, the assumption of no luminosity evolution can be and, for BLs, is relaxed.

We use parameter sets that give acceptable agreement to the EGRET data on blazar redshift and size distributions to make predictions that will be tested with GLAST,<sup>2</sup> and to estimate the blazar contribution to the EGRB. The connection of the properties of  $\gamma$ -ray blazars to blazars detected at radio, X-ray, and other wavelengths can be used to determine the accuracy of models that assume a radio/ $\gamma$ -ray connection.

Section 2 describes the sample of EGRET blazars used. The equations for the analysis are presented in Section 3, and results of the parameter study are described in Section 4. Predictions for GLAST and estimates for the EGRB from unresolved blazars are presented in Section 5, and we summarize in Section 6. Sensitivities of EGRET and GLAST to blazar flares, expressions for optimal sensitivities, and a discussion of a GLAST analysis strategy for blazar populations are given in the Appendix A. The self-absorption frequency is derived in Appendix B.

## 2. SAMPLE

Crucial to making a proper comparison of a model to EGRET blazar data is to choose a sample that is unbiased with respect to exposure and background. For example, exposure to the region around 3C 273 and 3C 279 was much longer than average over the lifetime of EGRET, so blazars found in these pointings would be detected to much smaller flux thresholds than on average. Likewise, blazars in the vicinity of the galactic plane would have to be much brighter than high-latitude sources to be detected above the diffuse galactic  $\gamma$ -ray

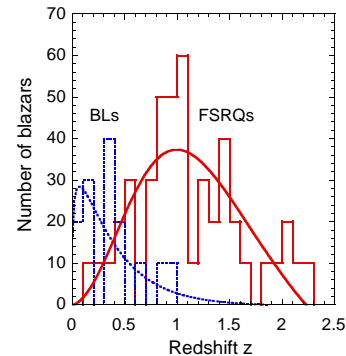


FIG. 1.— EGRET observations of the redshift distributions of blazars, separated into FSRQ (solid) and BL Lac (dotted) populations, are shown by the histograms. Smooth solid curve shows a monoparametric FSRQ blazar fit with BFR IR<sub>4</sub> (see Fig. 3),  $\Gamma = 10$ ,  $p = 3.4$ , EC statistics, and  $l'_e = 2.5 \times 10^{39}$  ergs s<sup>-1</sup> sr<sup>-1</sup>. The dotted curve shows the monoparametric blazar fit for the BL data for a blazar model with  $\Gamma = 4$ ,  $p = 3.0$ ,  $l'_e(z) = 6 \times 10^{42} z^{1.95}$  ergs s<sup>-1</sup> sr<sup>-1</sup>, synchrotron/SSC statistics, and  $\dot{n}_{BL}(z) \propto z^{-9/4}$ .

emission.

The 18 month all-sky EGRET survey (Fichtel et al. 1994), which ran from 1991 May to 1992 November, had roughly uniform exposure over all parts of the sky. Thirty-eight AGN identifications were reported in this catalog. Additional analysis of the Phase 1 data, as reported in the 3EG catalog (Hartman et al. 1999), revealed numerous additional detections of AGNs during Phase 1.

We have identified all the high-confidence blazars listed in the Third EGRET catalog that also appear during the 18 month all-sky survey, during which all parts of the sky receive roughly uniform exposure. The sample we use consists of 60 high-confidence gamma-ray blazars, consisting of 14 BLs and 46 FSRQs. We exclude sources within  $10^\circ$  of the Galactic plane, and use source catalogs (Padovani & Giommi 1995; Perlman 1996) to establish BL identifications. The integral photon number fluxes  $\phi(> E)$ , in units of ph( $>100$  MeV) cm<sup>-2</sup> s<sup>-1</sup>, were used to construct the FSRQ and BL size distributions.

Table 1 lists the sources from the Third EGRET catalog (Hartman et al. 1999) used in this study and their classifications. The  $\gamma$ -ray blazar sample, binned by redshift and grouped into BLs and FSRQs, is plotted in Fig. 1. Fig. 2 shows the FSRQ and BL size distributions. As shown in Appendix A, the on-axis EGRET sensitivity for a two-week pointing to high-latitude blazars is  $10^{-8} \phi_{-8}$  ph( $> 100$  MeV) cm<sup>-2</sup> s<sup>-1</sup>, with  $\phi_{-8} \cong 15$ . This is in accord with the dimmest blazars detected with EGRET during the two-week pointings. The corresponding  $\nu F_\nu$  threshold flux is  $f_\epsilon^{thr} = E^2 \phi_s(E)$ , where the source flux is given by eq. (A11). Thus

$$f_\epsilon^{thr} \cong 1.6 \times 10^{-12} (\alpha_{ph} - 1) \phi_{-8} \text{ ergs cm}^{-2} \text{ s}^{-1} \quad (1)$$

for measurements at  $E > 100$  MeV ( $\epsilon \gtrsim 200$ ), where  $\alpha_{ph}$  is the number spectral index. For  $\phi_{-8} \cong 15$ ,  $f_\epsilon^{thr} \cong 2.4 \times 10^{-11} (\alpha_{ph} - 1)$  ergs cm<sup>-2</sup> s<sup>-1</sup>, noting that  $\alpha_{ph} \cong (p+1)/2$  for Thomson, synchrotron, and SSC processes, where  $p$  is the number index of the assumed power-law electron distribution. As shown in Appendix A, an energy range that depends on the source spectral hardness should be used for optimal detection significance of blazars with GLAST or EGRET.

<sup>2</sup> glast.gsfc.nasa.gov, www-glast.stanford.edu

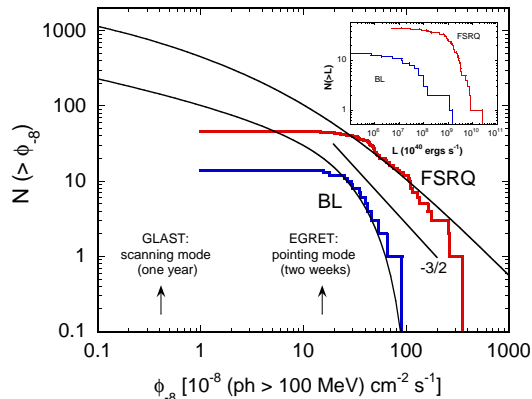


FIG. 2.— EGRET observations of the size distribution of blazars in terms of the integral photon fluxes at photon energies  $E \gtrsim 100$  MeV versus model size distributions for FSRQ and BL blazars, with parameters given in the caption to Fig. 1. Also shown are the integral flux sensitivities for EGRET in the pointing mode for a two-week observation (over  $\approx 1/24^{\text{th}}$  of the full sky) and for GLAST in the scanning mode for one year (over the full sky). The line labeled “ $-3/2$ ” has the slope of the size distribution of monoluminous sources uniformly distributed in flat space. The inset shows the size distribution of EGRET blazars in terms of apparent blazar luminosities in the energy range 100 MeV – 5 GeV.

The BLs and FSRQs display very different  $\gamma$ -ray properties. The BLs are less numerous and closer, with an average redshift  $\langle z \rangle \sim 0.37$ . For the FSRQs,  $\langle z \rangle \sim 1.11$ , with a tail on the FSRQ distribution reaching to  $z \sim 2.3$ . There are  $\approx 5\times$  as many FSRQs as BLs per unit peak flux in the EGRET range  $\phi_{-8} \approx 25 - 100$ . The FSRQs are  $\sim 1 - 2$  orders of magnitude more luminous than the BLs (inset to Fig. 2). The apparent powers of the FSRQs are as large as  $\approx 10^{50}$  ergs  $s^{-1}$ , compared to BLs, which are typically  $\lesssim 10^{48}$  ergs  $s^{-1}$ .

More detailed studies of the redshift and size distribution can be made with the EGRET data (R. Romani, private communication, 2006) based on surveys to identify  $\gamma$ -ray blazars (Sowards-Emmerd et al. 2005). These studies also show that the mean redshift of FSRQs is  $\gtrsim 1$ , and that both the BL and FSRQ populations have tails to high redshifts. The highest redshift  $\gamma$ -ray blazar candidate has  $z = 5.47$  (Romani et al. 2004). Thus we can be sure that the FSRQ BFR extends to at least  $z \gtrsim 5$ .

The Third EGRET catalog gives the two-week average fluxes for blazars during Phase 1. In comparison with models, the flaring timescale of the blazars is given by a rate density, which relates to the source density by a flaring timescale and duty cycle factor. We take this flaring timescale to be  $\approx 2$  weeks for the observer, and set the duty cycle equal to unity. If the duty cycle is less than unity, then the source space density must be greater, leaving the calculation of the intensity from unresolved sources independent of these factors.

### 3. ANALYSIS

We employ a simplified version of the standard model for blazars considered by Dermer & Gehrels (1995) (see also Sikora et al. 1997; Dermer & Davis 2000). A relativistically moving plasmoid ejected from a black-hole engine has accelerated within it, either through internal or external shocks or otherwise, a power-law distribution of quasi-isotropic ultra-relativistic electrons with number index  $p$ . In its proper frame, the plasmoid is as-

sumed to entrain a randomly oriented magnetic field with mean strength  $B$ . The nonthermal electrons emit synchrotron or Thomson radiation that is Doppler boosted by the effects of the relativistic motion. For the calculations shown here, we use the synchrotron beaming factor  $\propto \delta_D^{(5+p)/2}$  for synchrotron and synchrotron self-Compton (SSC) processes, where the Doppler factor  $\delta_D = [\Gamma(1 - \beta \cos \theta)]^{-1}$ , and the external Compton (EC) beaming factor  $\propto \delta_D^{3+p}$  (Dermer 1995), which also holds for scattering in the Klein-Nishina regime (Georganopoulos et al. 2001). Here  $\Gamma$  is the bulk Lorentz factor of the plasma blob,  $\beta = \sqrt{1 - \Gamma^{-2}}$ ,  $\alpha = (p-1)/2 = \alpha_{ph} - 1$  is the energy spectral index of the radiation, and  $\theta$  is the angle between the jet and line-of-sight directions. Continuous outflow scenarios produce a beaming pattern weaker by one power (Lind & Blandford 1985), but the single plasmoid approximation is more applicable to the flaring blazars.

#### 3.1. Cosmology of Nonthermal Sources

Consider a power-law distribution of electrons with low- and high-energy cutoffs, so that the total number distribution of nonthermal electrons within the plasmoid is described by

$$N'_e(\gamma) = K'_e \gamma^{-p} H(\gamma; \gamma_1, \gamma_2). \quad (2)$$

Note that  $p$  is the number index of the emitting electrons, and could be different from the injection index if cooling is important. Normalizing to the total comoving electron energy  $W'_e = m_e c^2 \int_1^\infty d\gamma \gamma N'_e(\gamma)$  implies

$$K'_e = \frac{(p-2)W'_e}{m_e c^2} (\gamma_1^{2-p} - \gamma_2^{2-p})^{-1} \rightarrow \frac{(p-2)W'_e \gamma_1^{p-2}}{m_e c^2}, \text{ when } p > 2, \gamma_2 \gg \gamma_1. \quad (3)$$

Cooling can introduce a break in the electron spectrum (Mücke & Pohl 2000), but the EGRET spectra of bright blazars are well fit by a single power law (Mukherjee et al. 1997), indicating that the single power-law approximation is adequate for a treatment of blazar statistics.

The  $\nu F_\nu$  nonthermal synchrotron radiation spectrum for a comoving isotropic power-law distribution of electrons entrained in a randomly oriented magnetic field is given in the  $\delta$ -function approximation by the expression

$$f_\epsilon^{syn} \cong \frac{\delta_D^4}{6\pi d_L^2} c \sigma_T U_B \gamma_s^3 N'_e(\gamma_s), \quad \gamma_s = \sqrt{\frac{\epsilon_z}{\delta_D b}}, \quad (4)$$

where the luminosity distance for a flat  $\Lambda$ CDM universe is

$$d_L(z) = \frac{c}{H_0} (1+z) \int_0^z dz' \frac{1}{\sqrt{\Omega_m(1+z')^3 + \Omega_\Lambda}}, \quad (5)$$

$U_B = B^2/8\pi$  is the magnetic-field energy density in the jet plasma,  $b \equiv B/B_{cr}$ , and  $B_{cr} = m_e^2 c^3 / e \hbar$  is the critical magnetic field.

The  $\nu F_\nu$  spectrum of jet electrons that Thomson scatter an external quasi-isotropic monochromatic radiation field with stationary (explosion)-frame dimensionless photon energy  $\epsilon_* = 10^{-4} \epsilon_{-4}$  and stationary frame

energy density  $U_*$  is

$$f_\epsilon^{EC} \cong \frac{\delta_D^6}{6\pi d_L^2} c\sigma_T U_* \gamma_C^3 N'_e(\gamma_C), \quad \gamma_C = \frac{1}{\delta_D} \sqrt{\frac{\epsilon_z}{2\bar{\epsilon}_*}} \quad (6)$$

(Dermer (1995); see Dermer & Schlickeiser 2002, for expressions describing the Thomson-scattered accretion-disk radiation fields). Restriction to the Thomson regime implies that  $\epsilon_z \lesssim 1/(8\bar{\epsilon}_*)$ , so that a target 5 eV UV radiation field would display effects from the onset of the KN decline in the cross section at  $E \gtrsim 6 \text{ GeV}/(1+z)$ . A more accurate treatment for GLAST analyses will have to consider the effects of the KN decline on the statistics.

The  $\nu F_\nu$  synchrotron self-Compton (SSC) radiation spectrum in the  $\delta$ -function approximation is

$$f_\epsilon^{SSC} \cong \frac{\delta_D^4}{9\pi d_L^2} \frac{c\sigma_T r_b U_B K_e'^2}{V_b'} \gamma_s^{3-p} \Sigma_C, \quad (7)$$

where the Compton-synchrotron logarithm  $\Sigma_c = \ln(a_{max}/a_{min})$ ,  $a_{max} = \min(b\gamma_2^2, \epsilon'/\gamma_1^2, \epsilon'^{-1})$ ,  $a_{min} = \max(b\gamma_1^2, \epsilon'/\gamma_2^2)$ , and  $\epsilon' = \epsilon_z/\delta_D$  (Gould 1979; Dermer et al. 1997). The SSC process has a similar dependence as the synchrotron process—though a curvature in the spectrum is produced by  $\Sigma_c$ —but with a different coefficient that depends on the physical size of the radiating plasma.

In this formulation, the radiating plasma is spherical in the comoving frame, with volume  $V_b' = 4\pi r_b'^3/3$ , where the blob radius

$$r_b' = \frac{ct_{var}\delta_D}{1+z} \lesssim \frac{2\Gamma ct_{var}}{1+z}, \quad (8)$$

and  $t_{var}(s) = 86400t(\text{day}) = 10^3 t_3$  is the measured variability time scale. For FSRQs measured with EGRET,

$$r_b' \lesssim \frac{2.6 \times 10^{16}(\Gamma/10)t(\text{day})}{(1+z)/2} \text{ cm} \simeq 0.01t(\text{day})(\Gamma/10) \text{ pc},$$

and for BLs measured with EGRET

$$r_b' \lesssim 2.4 \times 10^{14}(\Gamma/4)t_3 \text{ cm} \simeq 10^{-4}t_3(\Gamma/4) \text{ pc}.$$

For these blob sizes, the synchrotron radiation at GHz frequencies is likely to be heavily self-absorbed, as shown in Appendix B. This calls further into question the use of any radio/ $\gamma$ -ray correlation.

We rewrite eqs. (4) – (7) as

$$f_\epsilon^{proc} = \frac{l_e'}{d_L^2} \delta_D^q \epsilon_z^{\alpha_\nu}, \quad (9)$$

where  $\alpha_\nu = (3-p)/2$  is the  $\nu F_\nu$  spectral index, the directional comoving luminosity

$$l_e'(\text{ergs s}^{-1}\text{sr}^{-1}) = \frac{K_e' c\sigma_T}{6\pi} \begin{cases} U_{B_{cr}} b^{(p+1)/2}, & \text{syn} \\ \frac{K_e' \sigma_T}{2\pi r_b'^2} U_{B_{cr}} \Sigma_C b^{(p+1)/2}, & \text{SSC} \\ U_* (2\bar{\epsilon}_*)^{(p-3)/2}, & \text{EC} \end{cases} \quad (10)$$

the beaming factor index

$$q = \begin{cases} (p+5)/2, & \text{synchrotron, SSC} \\ p+3, & \text{EC} \end{cases},$$

and  $U_{B_{cr}} \equiv B_{cr}^2/8\pi$ .

The event rate per sr (or the directional event rate) for bursting sources in a  $\Lambda$ CDM cosmology is

$$\frac{d\dot{N}}{d\Omega} = \frac{c}{H_0} \int_0^\infty dz \frac{d_L^2(z) \dot{n}_{com}(z)}{(1+z)^3 \sqrt{\Omega_m(1+z)^3 + \Omega_\Lambda}}, \quad (11)$$

where  $\dot{n}_{com}(z)$  is the rate density of sources at redshift  $z$  (see Dermer 2006, for a detailed derivation). From the WMAP data (Spergel et al. 2003), we take  $\Omega_m = 0.27$ ,  $\Omega_\Lambda = 0.73$ , and Hubble's constant  $H_0 = 72 \text{ km s}^{-1} \text{ Mpc}^{-1}$ . The directional event rate (i.e., number count) of steady sources is

$$\frac{dN}{d\Omega} = \frac{c}{H_0} \int_0^\infty dz \frac{d_L^2(z) n_{com}(z)}{(1+z)^2 \sqrt{\Omega_m(1+z)^3 + \Omega_\Lambda}}, \quad (12)$$

and  $n_{com}(z)$  is the differential source density.

In an integral formulation for bursting sources (Dermer 1992), the observed directional event rate above the  $\nu F_\nu$  spectral flux threshold  $f_\epsilon^{thr}$  of the telescope is

$$\begin{aligned} \frac{d\dot{N}( > f_\epsilon^{thr})}{d\Omega} &= \frac{c}{H_0} \int_{f_\epsilon^{thr}}^\infty df_\epsilon \int_0^\infty dl_e' \int_{-\infty}^\infty dp \int_1^\infty d\Gamma \times \\ &\int_{-1}^1 d\mu \int_0^\infty dz \frac{d_L^2(z) \dot{n}_{com}(l_e', p, \Gamma; z)}{(1+z)^3 \sqrt{\Omega_m(1+z)^3 + \Omega_\Lambda}} \times \\ &\delta[f_\epsilon - f_\epsilon^{proc}(l_e', p, \Gamma, \mu)]. \end{aligned} \quad (13)$$

Here  $f_\epsilon^{proc}$  is the  $\nu F_\nu$  flux for the process under consideration, with synchrotron, EC, and SSC fluxes written as eq. (9),  $\mu = \cos\theta$ , and the blazar jet luminosity is characterized by  $l_e'$ . For a better treatment of detector response, one should calculate a photon-energy integration over effective area, rather than describing a  $\gamma$ -ray telescope by a  $\nu F_\nu$  flux sensitivity  $f_\epsilon^{thr}$  at a single photon energy  $\epsilon$ .

For mono-parameter  $\delta$ -function distributions of  $p$ ,  $\Gamma$ , and  $l_e'$ , we have

$$\begin{aligned} \frac{d\dot{N}( > f_\epsilon^{thr})}{d\Omega} &= \frac{2c}{H_0} \int_0^\infty dz \frac{d_L^2(z) \dot{n}_{com}(z)}{(1+z)^3 \sqrt{\Omega_m(1+z)^3 + \Omega_\Lambda}} \\ &\times \int_{-1}^1 d\mu \int_{f_\epsilon^{thr}}^\infty df_\epsilon \delta[f_\epsilon - f_\epsilon^{proc}(l_e', p, \Gamma, \mu)], \end{aligned} \quad (14)$$

where the various parameters specifying emission properties, for example,  $W_e'$ ,  $B$ ,  $r_b'$ , and  $U_*$ , are found in the directional power  $l_e'$ . In this expression, we include a factor of 2 for a two-sided jet.

### 3.2. Peak Flux and Size Distribution

It is trivial to perform the integration over  $df_\epsilon$  in eq. (14), which places a limit on the allowed values of  $\mu$ . Only values of cosine angle  $\mu \geq \hat{\mu}$  give detectable fluxes, where

$$\hat{\mu}(z, \Gamma, l_e', p, q, \epsilon, f_\epsilon) = \hat{\mu} = \frac{1}{\beta} \left[ 1 - \frac{1}{\Gamma} \left( \frac{l_e' \epsilon_z^{\alpha_\nu}}{d_L^2 f_\epsilon} \right)^{1/q} \right]. \quad (15)$$

The  $\nu F_\nu$  flux size distribution of blazars per sr per s is therefore given by

$$\frac{d\dot{N}}{d\Omega}(> f_\epsilon) = \frac{2c}{H_0} \int_0^\infty dz \frac{d_L^2(z) \dot{n}_{com}(z) [1 - \max(-1, \hat{\mu})]}{(1+z)^3 \sqrt{\Omega_m(1+z)^3 + \Omega_\Lambda}} \quad (16)$$

for two-sided blazar jet sources.

### 3.3. Redshift Distribution

The directional redshift distribution of sources with  $\nu F_\nu$  flux  $f_\epsilon > f_\epsilon^{thr}$  is simply given by

$$\frac{d\dot{N}}{dz d\Omega}(> f_\epsilon^{thr}) = \frac{2c}{H_0} \frac{d_L^2(z) \dot{n}_{com}(z)}{(1+z)^3 \sqrt{\Omega_m(1+z)^3 + \Omega_\Lambda}} [1 - \max(-1, \hat{\mu})]. \quad (17)$$

The threshold limitation prescribed by  $\hat{\mu}$  in eq. (15) now has  $f_\epsilon \rightarrow f_\epsilon^{thr}$ . The relation between  $f_\epsilon^{thr}$  and the integral photon number flux variable  $\phi_{-8}$  depends on  $p$  and  $\alpha_\nu$  as given by eq. (1).

### 3.4. Parameters

Eq. (9) shows that a  $\gamma$ -ray blazar can be detected from redshifts of order unity at the level  $f_\epsilon$  when the parameters satisfy the condition

$$f_\epsilon \cong l'_e \frac{\Gamma^q (2\epsilon)^{\alpha_\nu}}{d_L^2(z=1)} \quad (18)$$

which holds when  $\Gamma \gg 1$ . If a significant fraction of the EGRB originates from blazars, then  $p \cong 3.2$ . For synchrotron, SSC, or Thomson processes, this implies a photon number index  $\alpha_{ph} = 2.1$ , or  $\alpha_\nu = -0.1$ . EGRET observations of blazar spectral indices show that  $\alpha_{ph} = 2.03 \pm 0.09$  for BLs and  $\alpha_{ph} = 2.20 \pm 0.05$  for FSRQs, with an average spectral index of  $\alpha_{ph} = 2.15 \pm 0.04$  (Mukherjee et al. 1997). The evidence from EGRET that  $\alpha_{ph}$  is harder for BLs than for FSRQs means that the  $\nu F_\nu$  peaks of the  $\gamma$ -ray components of BLs are typically at higher energies than for FSRQs. Moreover, observations suggest that the flaring state spectra are harder than the quiescent emission, at least in the case of PKS 0528+134 (Mukherjee et al. 1996).

Taking  $\alpha_\nu = 0$  ( $p = 3$ ) and noting that  $d_L(z=1) \cong 2.0 \times 10^{28}$  cm, eq. (18) becomes

$$f_\epsilon \cong 2.5 \times 10^{-11} \left(\frac{\Gamma}{10}\right)^6 \left(\frac{l'_e}{10^{40} \text{ ergs s}^{-1} \text{ sr}^{-1}}\right) \text{ ergs cm}^{-2} \text{ s}^{-1} \quad (19)$$

for EC statistics. For synchrotron or SSC statistics,

$$f_\epsilon \cong 2.5 \times 10^{-11} \left(\frac{\Gamma}{10}\right)^4 \left(\frac{l'_e}{10^{42} \text{ ergs s}^{-1} \text{ sr}^{-1}}\right) \text{ ergs cm}^{-2} \text{ s}^{-1}, \quad (20)$$

so that a larger internal synchrotron power compared to Compton power is needed for the same  $\nu F_\nu$  flux when viewing within the beam of the jet.

In actual fitting of blazar statistical distributions, a degeneracy between  $\Gamma$  and  $l'_e$  is found that may partially be removed by obtaining limits on the bulk Lorentz factor  $\Gamma$  from  $\gamma\gamma$  attenuation arguments (e.g. Maraschi et al. 1992; Dermer & Gehrels 1995).

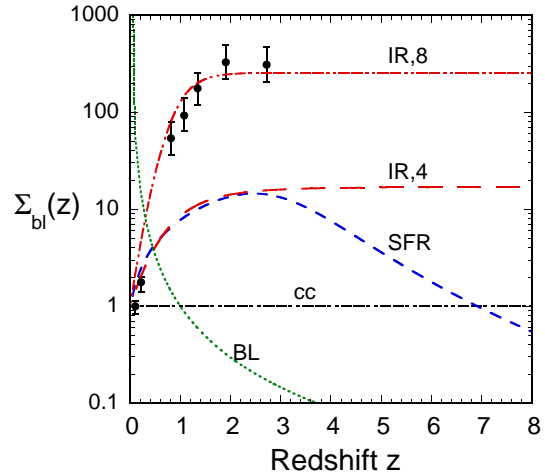


FIG. 3.— Model blazar formation rates (BFRs) used in this study. The curve labeled “cc” is the constant comoving rate, the curve “SFR” is the star formation rate from Hopkins & Beacom (2006), curve “IR,8” is eq. (25) with  $n = 8$  that is used to fit the IR luminosity density from IR luminous galaxies, curve “IR,4” is eq. (25) with  $n = 4$  used to fit FSRQ data, and curve “BL” is eq. (26) with  $a = 1.75$  used to fit to the BL data.

For standard FSRQ blazar parameters, we take

$$p = 3.4, \Gamma = 10, l'_e = 10^{40} \text{ ergs s}^{-1} \text{ sr}^{-1}, \quad (21)$$

and EC statistics. For standard BL blazar parameters, we take

$$p = 3.0, \Gamma = 4, l'_e = 10^{42} \text{ ergs s}^{-1} \text{ sr}^{-1}, \quad (22)$$

and syn/SSC statistics.

For two week ( $\approx 10^6$  s) observations,  $\approx 50$  flaring blazars were detected by EGRET above its  $\nu F_\nu$  threshold flux  $f_\epsilon^{thr} \cong 2.4 \times 10^{-11}$  ergs cm $^{-2}$  s $^{-1}$  over  $\approx 1$  year. Given the EGRET field-of-view (see Fig. 2), this implies a directional blazar flaring rate  $\approx 4$  sr $^{-1}$  Ms $^{-1}$ , implying a fiducial rate density  $\dot{n}_{com}(z=1)$  at redshift unity of about

$$4 \times 10^{-6} \text{ s}^{-1} \text{ sr}^{-1} \cong \frac{c}{H_0} 4 \times 10^{56} \text{ cm}^2 \dot{n}_{com}(z=1), \quad (23)$$

so that  $\dot{n}_{com}(z=1) \cong 0.8 \times 10^{-90}$  events cm $^{-3}$  s $^{-1}$ . Thus we expect that the blazar flaring rate density  $\dot{n}_{com} = 10^{-90}$  events cm $^{-3}$  s $^{-1} \approx 1$  event Gpc $^{-3}$  yr $^{-1}$ . The calculations for the local rate density of FSRQs give values larger by one or two orders of magnitude. The discrepancy can be resolved by considering the increased number of sources necessary to offset the reduction in the detection rate by  $\approx \Gamma^{-2}$  for the beamed blazar emission, and the different rate density at  $z \ll 1$  compared to  $z = 1$ , which depends on the form of the BFR.

### 3.5. Blazar Formation Rate Histories

The BFR functions are used to describe the change in the rate density of blazars through cosmic time. This does not mean that the comoving density of supermassive black holes changes, but rather that their flaring rate changes or their assignment to the FSRQ or BL class changes with time as a consequence of their definitions in terms of the optical emission line equivalent widths.

We consider the following BFRs  $\Sigma_{bl}(z)$ , shown in Fig. 3, which give the blazar comoving rate density  $\dot{n}_{com}(z) =$



$\Sigma_{bl}(z)\dot{n}_{com}$  in terms of the local comoving rate density  $\dot{n}_{com}$ :

1. Constant comoving rate density, so that  $\Sigma_{cc}(z) = 1$ . This form is employed for mathematical convenience.
2. Comoving rate  $\propto$  the blue/UV luminosity density, which is assumed to track the star formation rate (SFR) of the universe. We use the analytic form (Hopkins & Beacom 2006)

$$\Sigma_{SFR}(z) = \frac{1 + 6.78z}{1 + (z/3.3)^{5.2}}. \quad (24)$$

Blazar activity could be related to the SFR if stellar activity provides fuel for the supermassive black hole engine, for example, from material driven off by starburst nurseries encircling the nucleus (e.g., Haiman et al. 2004).

3. Comoving rate  $\propto$  sub-mm/far-IR luminosity density associated with luminous IR galaxies (Sanders 2004), which we fit using the analytic form

$$\Sigma_{IR,n}(z) = \frac{1 + 2^{-n}}{(1+z)^{-n} + 2^{-n}}. \quad (25)$$

We obtain a good fit to the data with  $n = 8$ , as shown in Fig. 3. If IR-luminous galaxies are caused by galactic merger events, as is indicated by morphological and spectral evidence (e.g., Sanders & Mirabel 1996, and references therein), this would connect blazars and the formation of supermassive black holes to galaxy collisions. Although related to supermassive black hole growth, the IR luminosity density does not, however, directly measure the activity of supermassive black holes, because the IR radiation is a convolution of the photon luminosity which is then reprocessed through thick columns of material. Hence we have generalized the form with a single adjustable parameter,  $n$ , that represents a range of BFR histories. The forms of  $\Sigma_{IR,8}$  and  $\Sigma_{IR,4}$  are shown in Fig. 3.

4. A BFR where the blazar flare rate density increases with cosmic time, which is found necessary to fit the BL data. The simple form considered is

$$\dot{n}_{BL}(z) = \frac{\dot{n}_{BL}(z=1)}{z^a}, \quad (26)$$

where  $a(> 0)$  is adjusted to fit the data. Because of the divergence in the rate density when  $z \rightarrow 0$ , this BFR has to be normalized at  $z > 0$ . The total blazar flaring rate is, however, a well-defined value when  $a < 3$ .

### 3.6. Diffuse Intensity

The apparently diffuse intensity from the superposition of emissions from many faint, unresolved blazars is given by (e.g., Dermer 2006)

$$\epsilon I_\epsilon = \frac{2c}{4\pi H_0} \int_0^\infty dz \oint d\Omega' \frac{\epsilon_*^2 q_{com}(\epsilon_*, \Omega'; z)}{(1+z)^2 \sqrt{\Omega_m(1+z)^3 + \Omega_\Lambda}}. \quad (27)$$

where  $\epsilon_* = \epsilon_z = (1+z)\epsilon$  and a factor of 2 is again introduced for two-sided jet sources. The direction vector  $\Omega'$  defines the direction of the jet axis with respect to the observer direction. This expression applies to persistent blazar sources, with comoving emissivity

$$\epsilon_*^2 q_{com}(\epsilon_*, \Omega'; z) = \frac{d\mathcal{E}_\gamma}{dt_* dV_{com} d\Omega'} = n_{com}(z) l'_e \delta_D^q \epsilon_z^{\alpha\nu}. \quad (28)$$

When sources are detected above threshold flux  $f_\epsilon^{thr}$ , they no longer contribute to the EGRB, as they are identified as a blazar source. This restricts eq. (27) only to those blazars with  $l'_e \delta_D^q \epsilon_z^{\alpha\nu} / d_L^2 < f_\epsilon^{thr}$ , leading to the following expression for the diffuse radiation from unresolved radio galaxies and black hole jet sources:

$$\epsilon I_\epsilon^{bl}(< f_\epsilon) \cong \frac{c\epsilon^{\alpha\nu}}{(q-1)H_0\beta\Gamma^q} \int_0^\infty dz \frac{(1+z)^{\alpha\nu-2}}{\sqrt{\Omega_m(1+z)^3 + \Omega_\Lambda}} \times n_{com}(z) l'_e(z) \{ [1 - \beta \min(1, \hat{\mu})]^{1-q} - (1+\beta)^{1-q} \}. \quad (29)$$

The dependence of this expression on  $f_\epsilon^{thr}$  is carried by  $\hat{\mu}$ , given by eq. (15).

Equating the EGRET two-week average fluxes with blazars that flare once in two weeks allows us to replace the comoving density of blazar AGN sources, given by

$$n_{com}(z)(\text{cm}^{-3}) \cong \frac{1.2 \times 10^6 \text{ s}}{1+z} \times \dot{n}_{com}(z) \text{ cm}^{-3} \text{ s}^{-1},$$

with the comoving rate density,  $\dot{n}_{com}(z)$ , of blazar flares. This replacement should be accurate to a duty cycle factor of order unity. Better studies based on GLAST observations will reveal the flaring behavior of  $\gamma$ -ray blazars; note that the threshold flux  $f_\epsilon^{thr,G}(t)$  for GLAST in the scanning mode is time-dependent when using eqs. (16) and (17) to fit the data.

## 4. RESULTS

Fig. 4 shows calculations of FSRQ blazar redshift distributions using the standard FSRQ blazar parameter set, eq. (21), with differences from the standard parameters as labeled. In this calculation, the detection threshold is  $\phi_{-8} = 15$ , corresponding to a  $\nu F_\nu$  flux threshold sensitivity, from eq. (1), of  $2.88 \times 10^{-12}$  ergs  $\text{cm}^{-2} \text{ s}^{-1}$  at  $\epsilon = 200$  for  $p = 3.4$ . Except for the light solid curves, which show results for a BFR given by the SFR history, eq. (24), FSRQ blazars are assumed to emit blazar flares in random directions with a constant comoving rate density. The local rate density,  $\dot{n}_{com}(z \ll 1)$ , is set equal to  $10^{-90} \text{ cm}^{-3} \text{ s}^{-1}$ .

The effect of increasing  $\Gamma$  or  $l'_e$ , of course, is to increase the distance from which blazars can be detected. Fig. 4a shows that the directional event rate per unit redshift is not greatly increased with increasing  $\Gamma$  factor, whereas this rate is increased with increasing  $l'_e$ . The reason for this is that by increasing  $\Gamma$ , the emission is jetted into a smaller solid angle, rendering a smaller fraction of the blazars visible, though from a larger distance. Nevertheless, the cumulative redshift distributions for different combinations of  $\Gamma$  and  $l'_e$  can be very similar, as seen in Fig. 4b. When  $\Gamma \gg 1$ , these two quantities enter into the threshold cosine angle  $\hat{\mu}$  according to the combination  $l'_e^{1/q}/\Gamma$  (eq. [15]), reflecting the degeneracy of the results as a function of these two quantities.

By changing the BFR function, the distribution of blazars with redshift can be adjusted to better agree with the observations. As is made clear by Fig. 4b, the effect of using the SFR function rather than the constant comoving rate is to decrease the number of low-redshift blazars, and to have more blazars detected at  $1 \lesssim z \lesssim 3$ .

Even though it is relatively simple to find a parameter set and BFR that gives a good fit to the FSRQ redshift distribution, it is considerably less simple to find a parameter set that gives a good fit to the joint redshift and size distribution. One difficulty in fitting the size distribution originates from sample incompleteness near the EGRET threshold. The value  $\phi_{-8} = 15$  applies to two-week observations of on-axis EGRET sources (Appendix A). Reduction in the effective area for off-axis sources means that the effective threshold where the EGRET sample is complete is larger than  $\phi_{-8} = 15$ . As a consequence, in the fitting of the data for FSRQs and BLs, the flux threshold was changed to  $\phi_{-8} = 25$  where the EGRET sample evidently no longer suffers from incompleteness. After adjusting the parameters and BFR histories, an acceptable fit to the FSRQ was obtained, as shown in Fig. 5.

This fit uses BFR IR,4 shown in Fig. 3, with parameter values shown in the figure caption. The value of  $p = 3.4$  was chosen to agree with the mean FSRQ photon spectral index  $\alpha_{ph} = 2.2$  (Mukherjee et al. 1997). The values of  $\Gamma$  and  $l'_e$  are not unique due to the degeneracy mentioned above, but the choice of  $\Gamma = 10$  is suggested by superluminal radio observations of FSRQs (Urry & Padovani 1995). As can be seen, the model fits the cumulative size distribution at  $\phi_{-8} > 25$  but not at lower values of  $\phi_{-8}$  due to sample incompleteness. The

FSRQ model gives a statistically acceptable fit to the distributions, noting that the Kolmogorov-Smirnov one-sided statistic for 46 sources (42 sources with  $\phi_{-8} = 25$ .) is 0.16 and 0.22 at the 90% and 99% confidence level, respectively. The model fit, does, however, show a slight deficit of blazars at  $1.5 \lesssim z \lesssim 2$  compared to the data. Moreover, the model somewhat overproduces the number of very bright FSRQs. Both the high-redshift deficit and overproduction of the brightest FSRQs could be alleviated by tuning the BFR to increase even faster than given by the model BFR, inasmuch as the brightest sources are generally found at lower redshifts. Given the statistically acceptable fit, further fine-tuning would, however, introduce additional parameters that are not well constrained.

Even after searching over a wide range of BFRs for the BLs, it was not found possible to obtain acceptable fits to the EGRET data for the joint redshift and size distributions of BLs. The difficulty was the very narrow range of peak fluxes, spanning less than a factor  $\approx 5$  from the dimmest to the brightest values (compared to a factor  $\approx 20$  for the FSRQs), and the requirement to have the same threshold integral photon flux  $\phi_{-8} = 25$ . The crux of the problem is that the blazar size distribution is steeper than  $-3/2$  (Fig. 2). A resolution of this problem was to introduce luminosity evolution of the BLs such that they dimmed with increasing time. At the same time, the comoving rate density of BLs increases with time, allowing for a large number of nearby BLs to be observed so that the redshift distribution of BLs could be fit. The effect of dimming luminosity and increasing rate density with time makes blazar fluxes over a narrow range of values.

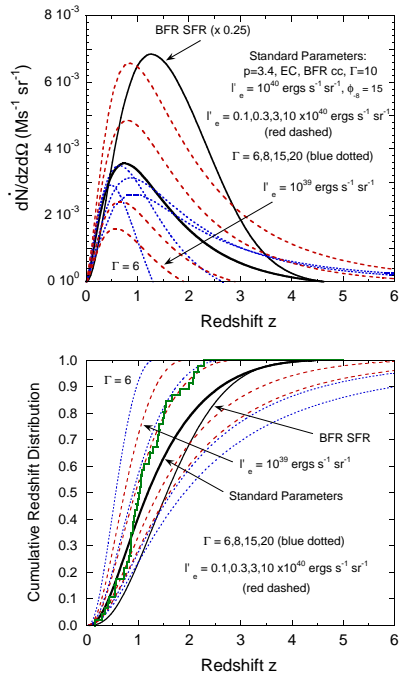


FIG. 4.— Parameter study of the redshift distribution of FSRQs, showing the effects of different parameter choices on the differential redshift distributions (top) and cumulative redshift distributions (bottom).

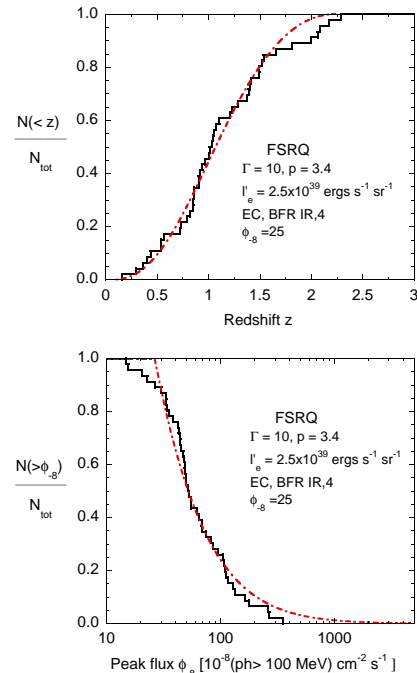


FIG. 5.— Smooth curves give model fits to the cumulative redshift and size distributions of FSRQ EGRET data, shown by the histograms in the top and bottom panels, respectively. Parameters for the fit are shown in the legend to the figure.

Fig. 6 shows the result of this procedure, using eq. (26) to describe the BFR of BLs, with  $a = 1.75$ , and luminosity evolution described by  $l'_e \propto z^{1.95}$ . We choose  $p = 2$  to agree with the mean BL photon spectral index  $\alpha_{ph} = 2.0$  (Mukherjee et al. 1997), which implies a threshold  $\nu F_\nu$  EGRET flux of  $f_\epsilon^{thr} = 4 \times 10^{-11}$  ergs  $\text{cm}^{-2} \text{s}^{-1}$  for  $\phi_{-8} = 25$ . Other parameters of this model are given in the caption to Fig. 6. The model gives a statistically acceptable fit, noting that in this case, the Kolmogorov-Smirnov one-sided statistic for 14 sources (12 sources for  $\phi_{-8} = 25$ .) is 0.275 and 0.39 at the 90% and 99% confidence level, respectively.

The sample of FSRQs and BLs with  $\phi_{-8} > 25$  suffers much less from sample incompleteness near threshold. This flux-limited sample has 4 fewer FSRQ and 2 fewer BL sources, and is therefore somewhat less constraining to the model fits. Although the fits to the size distribution using this smaller sample would be improved near threshold, the modified redshift distribution is not significantly changed, and the use of this sample does not change the conclusions of this study.

### 5. PREDICTIONS

Fig. 1 shows the fits to the FSRQ and BL redshift distributions implied by the models discussed in the previous section. The factors used to normalize the flaring rates give a local FSRQ flare rate density equal to

$$\dot{n}_{FSRQ} \cong 5.66 \times 10^{-88} \text{ cm}^{-3} \text{ s}^{-1} \cong 17 \text{ Gpc}^{-3} \text{ Ms}^{-1} \cong 1.7 \times 10^{-8} \text{ Mpc}^{-3} \text{ Ms}^{-1} \quad (30)$$

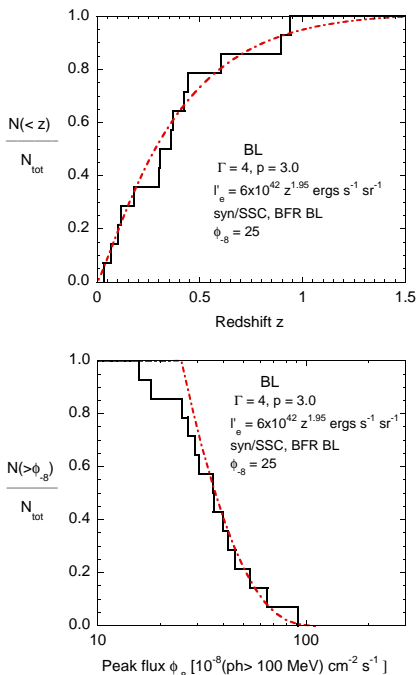


FIG. 6.— Smooth curves give model fits to the cumulative redshift and size distributions of BL EGRET data, shown by the histograms in the top and bottom panels, respectively. Parameters for the fit are shown in the legend to the figure. The rate-density dependence of the BL Lac flares is  $\propto z^{-1.75}$ .

for FSRQs, and a comoving BL flare rate density at  $z = 1$  equal to

$$\dot{n}_{BL}(z = 1) \cong 1.23 \times 10^{-88} \text{ cm}^{-3} \text{ s}^{-1} \cong 3.6 \text{ Gpc}^{-3} \text{ Ms}^{-1} \cong 3.6 \times 10^{-9} \text{ Mpc}^{-3} \text{ Ms}^{-1} \quad (31)$$

for BLs. The predicted size distributions of FSRQs and BLs extrapolated to small values of  $\phi_{-8}$  implied by the model are shown by the solid curves in Fig. 2. Also shown is the one-year sensitivity of GLAST in the scanning mode, which is at the level of  $\approx 0.4 \times 10^{-8} \text{ ph}(> 100 \text{ MeV}) \text{ cm}^{-2} \text{ s}^{-1}$ . The model fit predicts that GLAST will detect  $\approx 700$  FSRQs and FR2 radio galaxies, and  $\approx 160$  BLs and FR1 radio galaxies after one year of observation, and an additional  $\approx 200$  dim FSRQs/FR2 galaxies and  $\approx 50$  more BLs/FR1 galaxies after 3 more years of observation. These numbers should be taken with an estimated uncertainty less than a factor-of-2, considering our lack of knowledge of blazar activity at  $z \gtrsim 3$ . The predicted numbers would represent a lower limit if there are blazar subclasses yet to be discovered that are numerous. Broadening of the luminosity and  $\Gamma$  distributions might increase the total number, though by only factor of order unity. Additional classes of low luminosity blazars that were not detected with EGRET could be discovered with GLAST, and these would produce an upturn in the size distribution at low fluxes. The number of such sources are, of course, limited by the level of the EGRB.

Fig. 7 shows the predicted FSRQ and BL blazar redshift distributions for GLAST. The distribution predicted for EGRET is shown by the dashed curves, corresponding to the result shown in Fig. 1, and the predicted distributions for GLAST sensitivities of 1, 3, 10, 30, and 100 $\times$  the EGRET sensitivity of  $\phi_{-8} = 15$  are shown by the solid curves.

Fig. 8 shows the contribution to the EGRB as reported by the EGRET team (filled data points; Sreekumar et al.

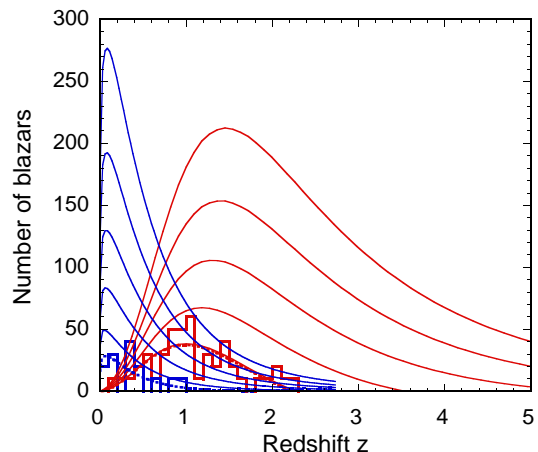


FIG. 7.— Histograms show the redshift distributions of FSRQs and BLs discovered with EGRET. Dotted curves show the model fits to the distributions, using detection characteristics typical of EGRET (and  $\phi_{-8} = 25$ ; see Fig. 1). Solid curves show the predicted FSRQ and BL redshift distributions using the parameters used to model the EGRET data, though with detection characteristics of GLAST. For the GLAST predictions, the observing photon energy is set equal to 1 GeV ( $\epsilon \approx 2000$ ), and the detection sensitivity is 1, 3, 10, 30, and 100 $\times$  better than EGRET, using the  $\phi_{-8} = 15$  as the flux threshold for EGRET.



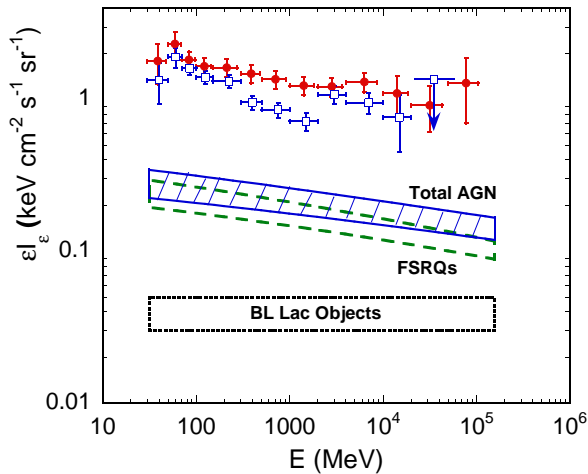


FIG. 8.— The intensity of the isotropic EGRB measured with EGRET is shown by the filled data points (Sreekumar et al. 1998), and the EGRB after subtraction of a component of quasi-isotropic galactic  $\gamma$  radiation is shown by the open data points (Strong et al. 2004). The dashed box gives the diffuse intensity from unresolved FSRQs, and the dotted box give the diffuse intensity from unresolved BLs, and the curve labeled “Total AGN” is the sum of the two. The boundary of the box represents the flux limit below which blazars are assumed to be unresolved, and correspond to the range for  $\phi_{-8} = 25$  and  $\phi_{-8} = 12.5$ .

1998), and as derived from the EGRET data using the GALPROP cosmic-ray propagation code (open data points; Strong et al. 2000, 2004). The boxes give the contributions to the EGRB from unresolved FSRQs and BLs with flux values between  $\phi_{-8} = 25$ , below which a two-week observation is incomplete, and  $\phi_{-8} = 12.5$ . This latter value is a factor of two less than the brighter value, and is chosen because EGRET had an effective lifetime of  $\approx 4$  years in terms of its capability during the first year, due to limited amount of spark chamber gas. This would produce a factor  $\approx 2$  better sensitivity before sample incompleteness dominates. Nonuniformity in exposure and angle to the normal of EGRET suggests that the threshold is in fact quite broad.

The steeper FSRQ and flatter BL spectra in Fig. 8 arise from using  $p = 3.4$  for FSRQs and  $p = 3$  for BL Lacs (note also the weak curvature in the calculated FSRQ background spectrum). The model results imply that the total AGN (BL+FSRQ) contribution to the EGRB as measured by Sreekumar et al. (1998) is at the level of  $\approx 12 - 20\%$ , and has a spectral index remarkably similar to the index measured in the EGRET analysis. The FSRQ contribution to the EGRET  $\gamma$ -ray background at 1 GeV is estimated at the level of  $\approx 10 - 15\%$ , and the BL contribution is  $\approx 2\% - 4\%$ . This contribution also includes FR1 radio galaxy, estimated by Stawarz et al. (2006) as contributing at the  $\approx 1\%$  level ( $\approx 6 \times 10^{-3}$  keV cm $^{-2}$  s $^{-1}$  sr $^{-1}$ ). The other sources classes that contribute to the residual EGRB are considered elsewhere (Dermer 2006). Note that no hard component BL Lac contribution to the EGRB is calculated here, though one must exist given measurements of hard-GeV spectrum BL Lac objects (e.g., Kataoka et al. 1999; Petry et al.

2000, for Mrk 501, which is not in our sample). Spectral hardening during flaring is also not considered here. Even so, this calculation implies that there is room for a number of other sources and/or source classes to make up the EGRB.

## 6. DISCUSSION

We have employed a simple physical model to fit population statistics of EGRET  $\gamma$ -ray blazar data and make predictions for the data anticipated from GLAST. By characterizing all FSRQs and BLs in terms of single values of  $\Gamma$  and  $l'_e$ , the model contains the fewest number of free parameters while still agreeing with the basic physical understanding of blazars as a two-sided jet of collimated relativistic plasma outflow with the radiation Doppler boosted by the motion of the jet. Other than blazar rate density evolution, described in terms of the BFR function, only the parameters  $\Gamma$ , the proper directional power  $l'_e$ , the power law index  $p$  and beaming statistic  $q$  define a model. The values of  $p$  and  $q$  are known with some certainty from observations. The model is further simplified in that the cumulative distributions are degenerate in the quantity  $l'_e{}^{1/q}/\Gamma$  when  $\Gamma \gg 1$ .

We have used  $\Gamma \cong 10$  for FSRQs and  $\Gamma \cong 4$  for BLs. These values of  $\Gamma$  are generally consistent with Lorentz factors inferred from fits to the local luminosity functions of radio galaxies and blazars (Urry & Padovani 1995) and measurements of superluminal motions (Vermeulen & Cohen 1994). The superluminal motion observations indicate that BLs have smaller Doppler factors on average than FSRQs, though in both cases the spread in Doppler factors is rather large (Jorstad et al. 2001). Good fits to the FSRQ data are obtained with parameters  $\Gamma = 10$ ,  $l'_e = 2.5 \times 10^{39}$  ergs s $^{-1}$  sr $^{-1}$ ,  $p = 3.4$ , and the EC beaming statistic. A BFR function that increases by a factor 10 – 20 from  $z \ll 1$  to  $z \approx 1 - 2$  was required to jointly fit the FSRQ redshift and size distribution, but a good fit was obtained even without luminosity evolution.

In contrast, it was not found possible to obtain a good fit to the BL redshift and size distributions without also invoking luminosity evolution. The BL size distribution declines more rapidly than a uniform Euclidean size distribution  $N(> \phi) \propto \phi^{-3/2}$ , as can be seen in Fig. 2. Any luminosity function, whether a kinematic luminosity function produced by the randomly oriented blazar jets, or a luminosity function given in terms of a range of jet powers, only flattens the size distribution. A feasible solution to this dilemma was to have the BL luminosity dim with time while the rate density of BL flares increases with time. A model that provides a reasonable fit to the BL data has  $\Gamma = 4$ ,  $l'_e(z) = 6 \times 10^{42} z^{1.95}$  ergs s $^{-1}$  sr $^{-1}$ , a rate density evolution of BLs  $\propto z^{-9/4}$ ,  $p = 3.0$ , and the synchrotron/SSC beaming statistic.

Before proceeding to the implications of this analysis, a few points should be made.

1. The tightly constrained parameter space in this simplified blazar model leads to fairly robust predictions for the number and intensity of blazars, and we think that the number of blazars and radio galaxies cannot be more than a factor-of-two in error, and then in the direction of more sources and

greater AGN background  $\gamma$  rays. A more precise error analysis must be considered in further study of this model.

2. Luminosity evolution was introduced in the BL fitting, but not the FSRQ fitting. The blazar's power evolves with cosmic times, reflecting the growth of the supermassive black hole (including binary black-hole merger episodes) and its intermittent fueling. The jet power is related to the accretion power in ways not fully understood, and is likely also dependent on black-hole spin. Modeling FSRQ growth and fueling with only a BFR function is possible with the EGRET data, but may well fail when modeling the larger and more meaningful GLAST data set. The next step in the analysis effort is to allow luminosity evolution of both FSRQs and BLs based on a physical model for supermassive black-hole growth and fueling, including duty factors on small and large timescales.
3. The quality of the fits, though acceptable, is not as good as in the study of Mücke & Pohl (2000). This indicates that a range of luminosities or injection energies may be required to obtain the best fits for the FSRQs, and that the form of the  $\gamma$ -ray luminosity function may be well represented by the luminosity function of FR1 and FR2 radio galaxies. Note also that the BL sample used in the Mücke & Pohl (2000) appears smaller and less constraining than the BL sample used here. The size distributions of BLs measured with GLAST will show whether the BL sample used in this study is representative.

### 6.1. Blazar evolution

The solution presented here that fits both the steep BL size distribution and the BL redshift distribution was to have joint *positive* luminosity evolution and *negative* source density evolution. From a simple size-distribution analysis in the Euclidean limit, the flux ( $\phi$ ) dependence of the integral size distribution goes as

$$N(> \phi) \propto \phi^{-(3-a_n)/(2-a_l)},$$

where  $l'_e \propto z^{a_l}$  and  $n(z) \propto z^{-a_n}$ , and  $a_n = 0$  for a uniform distribution of sources. A flatter (steeper) size distribution occurs for negative (positive) luminosity evolution with  $a_l < (>)0$ . Arranging to fit not only the BL size distribution with slope steeper than the uniform Euclidean value of  $-3/2$  requires positive luminosity evolution, and also to fit the measured BL redshift distribution required negative source rate-density evolution, leading after trial and error to the result  $a_l = 1.95$  and  $a_n = 9/4$ . Recalling the definition of  $\langle V/V_{max} \rangle$  as the normalized sum over the test statistic  $(\phi_i/\phi_{thr})^{-3/2}$ , one sees that size distributions steeper than  $-3/2$  have a larger number of faint detections near threshold than for a uniform Euclidean distributions and thus have  $\langle V/V_{max} \rangle > 0.5$ ; size distributions flatter than  $-3/2$  have a deficit of faint detections near threshold and thus have  $\langle V/V_{max} \rangle < 0.5$ .

This EGRET BL analysis indicates that  $\langle V/V_{max} \rangle > 0.5$ , similar to the case for bright 1 Jy radio sources or the brightest BL Lac objects selected at X-ray energies (Giommi et al. 2001). From Fig. 2, we predict that

$\langle V/V_{max} \rangle$  for BLs will shift to  $< 0.5$  within a few months of the start of GLAST measurements, as fainter BL Lac objects and FR1 radio galaxies will be lost due to cosmological effects and the small number of high-redshift BLs. Our analysis leads, however, to very different conclusions than obtained previously when considering only the size distribution and  $\langle V/V_{max} \rangle$  value from various BL surveys at radio and X-ray energies. For example, a flatter than  $-3/2$  size distribution is found in the ROSAT (0.5 – 2.0 keV) all-sky survey (RASS) of over 30 BL Lac objects complete to  $f_x(0.5 - 2.0 \text{ keV}) > 8 \times 10^{-13} \text{ ergs cm}^{-2} \text{ s}^{-1}$  (Bade et al. 1998), corresponding to a deficit of sources near threshold, or negative BL luminosity evolution. The same conclusion is found by Giommi et al. (1999), who assemble a sample of 155 BL Lacs by cross correlating the RASS survey results with radio sources from the NRAO VLA Sky Survey. The resulting radio luminosity size distribution of these X-ray selected BL Lac objects also exhibit a negative BL evolution. Rector et al. (2000) measured redshifts and analyzed sources in the Einstein 0.3 – 3.5 Medium Sensitivity Survey, and obtained  $\langle V/V_{max} \rangle \cong 0.4$ , again showing a deficit of near threshold sources compared to the uniform, Euclidean expectation.

It is meaningful to interpret a flattening of the size distribution compared to a  $-3/2$  slope as a reduction in luminosity at early times (Padovani & Giommi 1995). Here however we additionally require, as do Mücke & Pohl (2000), that the redshift distribution is also accurately fit with the same model that fits the size distribution. Unlike the Giommi et al. (2006) calculation of the EGRB from  $\gamma$ -ray blazars, no radio/ $\gamma$ -ray connection is assumed throughout this analysis (though radio data is used to guide the choices of  $\Gamma$ ). The results from joint fitting of EGRET data are severely constraining: the comoving rate density of FSRQ declines by a factor  $\gtrsim 10$  at  $z \ll 1$  compared to  $z \lesssim 1 - 2$ , while the rate density of BLs rapidly increases for  $z \ll 1$  and, at the same time, the mean luminosity of BL flares declines with time.

This behavior is in striking accord with the scenario (Böttcher & Dermer 2002; Cavaliere & D'Elia 2002) linking BLs to FSRQs through an evolution in declining accretion rates and increasing black hole masses. In the particular formulation of Böttcher & Dermer (2002), the reduction in the amount of gas and dust that both fuels the central black hole engine and scatters accretion-disk radiation causes a transformation of the FSRQs into the BLs in terms of spectral properties, thereby explaining the blazar sequence correlating  $\nu F_\nu$  peak synchrotron frequencies and apparent synchrotron power (Sambruna et al. 1996; Fossati et al. 1998), and puts on a more physical basis the correlations between the peak synchrotron frequency, peak electron Lorentz factor, and injection and external radiation compactnesses proposed by Ghisellini et al. (1998) to explain the blazar sequence. Cavaliere & D'Elia (2002) argue that the mean luminosity of the BLs does not change much over several gigayears, and that the flattened size distribution of BLs at low fluxes stem from negative density evolution, with spectral differences associated with transition from accretion power to a component from the black-hole spin.

A clearcut prediction of this scenario is that the mean

masses of black holes in BLs is larger than that in FSRQs at the same epoch. The minimum variability timescale of blazar flares should be proportional to black hole mass (§A.5), but the shorter timescale flaring behavior of BL Lacs measured with Whipple and HESS compared with the minimum variability timescale of FSRQs measured with EGRET is opposite to the expected behavior, but may only reflect sensitivity limitations of EGRET. Probably there is flaring on every timescale, and a power spectral density analysis is required to see if there is a size scale where temporal power declines, corresponding to the black hole mass. This question will obviously be subject to extensive investigation with GLAST.

Ghisellini & Celotti (2001) infer the black hole masses of FR1 and FR2 radio galaxies on the basis of an expression for the central black hole mass in terms of host galaxy absolute R-band magnitudes. Relating jet power to radio luminosity suggests that FR1 galaxies are low Eddington-ratio ( $\lesssim 10^{-2}$ ) and FR2 galaxies are moderate Eddington-ratio (0.01 – 0.1) sources. There is a tendency for the FR1 galaxies to have larger black-hole masses than FR2 galaxies, but this effect is too weak to provide an unambiguous test of the  $FSRQ \rightarrow BL$  evolutionary scenario.

It is unphysical to extend the form of the BL rate density evolution,  $\propto z^{-9/4}$ , to arbitrarily small redshifts. The comoving density of FSRQs forming at high redshifts should equal the comoving density of the BLs at low redshifts in the picture of  $FSRQ \rightarrow BL$  evolution considered here. The BL density will saturate at  $z_{bl}$  when all FSRQs have converted into BLs. If the duty cycle of the two sources classes is similar, this occurs at  $\dot{n}_{BL}(z_{bl}) \cong \dot{n}_{FSRQ}(z \gtrsim 1)$ . Using the derived values in eqs. (30) and (31) and the BFR functions, this takes place at  $z_{bl} \cong 0.1$ . Modifying the BL BFR to be constant at  $z \leq z_{bl}$  has minimal effects on the results, but should be considered in the next step of the analysis.

### 6.2. Space density of blazars

The local density of blazar sources given from this analysis can be compared with the space density of blazar host galaxies, namely early-type elliptical galaxies. From a K-band survey of bright galaxies with  $z \lesssim 0.4$ , Huang et al. (2003) calculate a local galaxy density of  $0.0048 \pm 0.001 \text{ Mpc}^{-3}$  for galaxies of all types with  $h = 0.72$ . The density of early-type galaxies is  $\approx 10\%$  of the total, or  $\approx 5 \times 10^{-4} \text{ Mpc}^{-3}$ . In comparison, the comoving densities of the sources of FSRQ and BL flares are  $n_{FSRQ}(z \ll 1) \cong 2 \times 10^{-8} \text{ Mpc}^{-3}$  and  $n_{BL}(z = 1) \cong 2 \times 10^{-9} \text{ Mpc}^{-3}$ , assuming a duty factor equal to unity (a duty factor less than unity implies a proportionately smaller source density).

The comoving density of sources at the present epoch is, in the scenario where FSRQs evolve into BLs, equal to  $\approx \Sigma_{FSRQ}(z \gg 1)n_{FSRQ}(z \ll 1) \cong 17n_{FSRQ}(z \ll 1) \cong 4 \times 10^{-7} \text{ Mpc}^{-3}$ . This is about three orders of magnitude smaller than the elliptical galaxy density. Either only a small fraction of ellipticals host radio galaxies, or the duty cycle of elliptical galaxies that harbor radio and  $\gamma$ -ray jets is a small fraction of the total lifetime of the source (see Haiman et al. 2004, for more speculations).

## 7. SUMMARY AND CONCLUSIONS

A method to analyze the population statistics of  $\gamma$ -ray blazars solely from the  $\gamma$ -ray data was considered in this paper (see also Mücke & Pohl 2000). By performing the  $\gamma$ -ray population study independent of other wavebands, the reliability of this method to other methods that invoke a radio/ $\gamma$ -ray correlation can be tested, and the physical reasons for differences in radio galaxy and blazar populations selected from observations at different wavebands can be explored.

Although a radio/ $\gamma$ -ray correlation was avoided, guidance to assign values of  $\Gamma$  was taken from radio observations. Measurements of apparent superluminal motion from radio observations on the scale of  $\approx 0.1 - 1 \text{ pc}$  from the black hole imply  $\Gamma$  factors. The  $\gamma$  rays may originate from within hundreds to thousands of Schwarzschild radii of the supermassive black hole, so that the  $\Gamma$  values derived from radio observations may not be appropriate to the analysis of  $\gamma$ -ray data. Radio observations suggest that  $\gamma$ -ray flares could originate from the same physical scale as the superluminal blobs (Jorstad et al. 2001a), though spectral modeling of some X-ray selected BLs such as Mrk 421 and Mrk 501 suggest larger Doppler factors  $\approx 50$  (Krawczynski et al. 2001, but see Georganopoulos & Kazanas (2003); Ghisellini et al. (2005) for possible resolutions to this puzzle) than inferred from superluminal motion observations. Lower limits to the values of  $\Gamma$  for BLs and FSRQs will be inferred from  $\gamma\gamma$  attenuation arguments applied to the GLAST observations. This will not only provide better values to use for modeling the population statistics of  $\gamma$ -ray blazars, but will help break the parameter degeneracy in the modeling.

By avoiding an underlying radio/ $\gamma$ -ray assumption, only a very simplified blazar model could be investigated. This model nevertheless contains the essential blazar physics, and can be simply generalized to include a range of  $\Gamma$  factors and an evolving, broadened luminosity function. For the analysis of the EGRET data, introducing distributions in  $\Gamma$  or  $l'_e$  would allow too large a parameter space to explore without introducing some radio/ $\gamma$ -ray connections, so we considered fixed values of  $\Gamma = 10$  for FSRQs and  $\Gamma = 4$  for BLs, and found values of luminosity  $l'_e$  that gave reasonable fits to the data. Because mean spectral indices were assigned from  $\gamma$ -ray observations, and the beaming factor statistic was taken from blazar physics, only the value of  $l'_e$ , the BFR function and, when necessary, the redshift dependence of  $l'_e$ , were varied in order to fit the EGRET redshift and size distributions.

Within these constraints, the EGRET data for FSRQs was fit with a BFR function that had  $\approx 10\times$  more sources at  $z = 1$  than at present, which could be related either to a star-formation rate function or an evolutionary behavior proportional to the far IR/sub-millimeter luminosity density related to IR radiation (Sanders 2004; Błażejowski et al. 2000). The EGRET data for BLs could not be fit by only modifying the form of the BFR, and luminosity evolution was also required. The resulting solution—that the density of BLs increase and their mean jet powers dim with time—is in accord with the scenario where FSRQs evolve from BLs.

The analysis implies that the contribution of unresolved blazars to the extragalactic  $\gamma$ -ray background measured with EGRET (Sreekumar et al. 1998) at the

level of  $\approx 20\%$  at 1 GeV, leaving room for various source classes or additional types of blazars, such as hard GeV-spectrum blazars, to which EGRET was not very sensitive. Approximately 1000 blazars are predicted from this analysis to be discovered with GLAST during its first year of operation, but this could be an underestimate for the reason just stated, though not by more than a factor of 2. As also observed with EGRET, the BL/FR1  $\gamma$ -ray sources are predicted to have a much smaller mean redshift than the FSRQ/FR2 sources (Fig. 7). The predictions for the high redshift ( $z \gtrsim 3 - 5$ ) blazar population is very uncertain because of the very few high- $z$   $\gamma$ -ray blazars observed with EGRET. If blazars only make  $\approx 20\%$  of the EGRB at 1 GeV, then star-forming galaxies, starburst galaxies, and cluster of galaxies are likely to contribute a significant fraction of the difference, so we can expect GLAST to discover new  $\gamma$ -ray source classes.

With the much larger data set from GLAST, more detailed analyses will allow various effects related to

blazar spectra and flaring and the evolutionary connections between various classes of cosmological black-hole jet sources to be examined in much greater detail.

I thank Stanley P. Davis for helping assemble the sample used in the analysis. I would also like to thank J. Chiang, S. Ciprini, B. Dingus, G. Fossati, P. Giommi, T. Le, G. Madejski, J. McEnery, F. C. Michel, and R. Romani for useful comments and discussions that influenced this work. Thanks are also due to B. Lott, P. Michelson, and S. Ritz for encouragement, to P. Sreekumar for providing the EGRET data for the diffuse  $\gamma$ -ray background, and particular thanks to A. Reimer and the anonymous referee for many helpful comments and useful suggestions. The work of C. D. D. is supported by the Office of Naval Research and GLAST Interdisciplinary Science Investigator grant DPR S-13756G.

## APPENDIX

### SENSITIVITY OF EGRET AND GLAST TO BLAZAR FLARES

We follow the approach of Dermer & Dingus (2003). The properties of a  $\gamma$ -ray imaging spark chamber or silicon tracker detector depends on its shower pattern, assumed to be described by a Gaussian with 68% containment angle  $\hat{\theta}$  and energy-dependent angular point spread function (psf) described by

$$\theta_{psf} = \hat{\theta} u^{-w}, \quad (\text{A1})$$

where the photon energy in units of 100 MeV is

$$u = \frac{E}{E_{100}} \text{ and } E_{100} = 100 \text{ MeV}. \quad (\text{A2})$$

For EGRET,  $\hat{\theta} \cong 5.7^\circ/57.3^\circ \cong 0.1$  and  $w = 1/2$ . For GLAST,  $\hat{\theta} \cong 3.5^\circ/57.3^\circ \cong 0.06$  and  $w = 2/3$ .

The effective area  $A(E, \theta, \phi)$  depends on photon energy  $E$ , angle  $\theta$  from zenith, and azimuthal angle  $\phi$  measured with respect to the zenith angle, according to

$$A(E, \theta, \phi) \cong A(u) \cong A_0 u_0^a, \quad (\text{A3})$$

where  $A_0$  is the effective area averaged over the field of view, defined as the opening solid angle within which the effective area is 50% of the on-axis FOV. The FOV of EGRET is  $\cong 4\pi/24 \cong 0.5$  sr, and the FOV of GLAST is  $\cong 4\pi/6 \cong 2$  sr. The parameters describing the effective area  $A_0$  at 100 MeV and index  $a_0$  are, respectively,  $\cong 1200$  cm<sup>2</sup> and  $a_0 \cong 0$  for EGRET, and  $\cong 6200$  cm<sup>2</sup> and  $a_0 \cong 0.16$  for GLAST.<sup>3</sup>

The significance to detect a signal at the  $n\sigma$  level is given by

$$n \cong \frac{S}{\sqrt{\alpha S + (1 + \alpha)B}} \quad (\text{A4})$$

(Li & Ma 1983, eq. 9), where  $S$  is the number of source counts,  $B$  is the number of background counts, and  $\alpha = t_{on}/t_{off}$  is the ratio of on-source to off-source observing times. If the background is precisely known,  $\alpha \rightarrow 0$ , and

$$n \cong \frac{S}{\sqrt{B}}. \quad (\text{A5})$$

In the limit  $\alpha \ll 1$  and  $n \gg 1$ , eqs. (1) and (2) overestimate the fluctuation probability compared to a maximum likelihood expression confirmed by Monte Carlo simulations (Li & Ma 1983), so eq. (A5) should be a conservative expression for the detection significance.

### Background Counts

We assume that the source location is precisely known. The number of background photons within solid element  $\Delta\Omega(E)$  centered in the direction  $\vec{\Omega}$ , and with energies  $> E_1$  observed during an observing time  $\Delta t$  is

$$B(> E_1) \cong \int_0^{\Delta t} dt \int_{E_1}^{\infty} dE \Delta\Omega(E) A[E, \theta(t), \phi(t)] \Phi_B(E, \vec{\Omega}). \quad (\text{A6})$$

<sup>3</sup> These satisfy the GLAST Science Requirements Document; the actual performance is given at the GLAST websites. Note that the estimate requires an average over the FOV.

The background photon flux per steradian,  $\Phi_B(E, \vec{\Omega}) = dN_\gamma/dAdtd\Omega dE$ , is assumed to be time-independent; thus this treatment excludes passage through the South Atlantic Anomaly. This expression also applies to time-independent diffuse backgrounds, not time-variable point sources or variable backgrounds. The effective area  $A[E, \theta(t), \phi(t)]$  of the telescope at energy  $E$  changes for a source at time-varying angles  $\theta$  and  $\phi$  with respect to the telescope  $\hat{z}$ -axis, which change with time due to rocking or slewing or Earth occultation. These effects are taken into account with an exposure factor  $X$ . Note that eq. (A6) assumes that each photon count can be precisely assigned an energy  $E$  and direction  $(\theta, \phi)$ .

The apparently diffuse isotropic  $\gamma$ -ray background spectrum is independent of  $\vec{\Omega}$  and is given by Sreekumar et al. (1998) as

$$\Phi_X(E) = k_x u^{-\alpha_B}, \quad (\text{A7})$$

where  $k_x = 1.73 \pm 0.08 \times 10^{-7}$  ph (cm<sup>2</sup>-s-sr-MeV)<sup>-1</sup> and  $\alpha_B = 2.10 \pm 0.03$ . This expression is a valid description of the minimum  $\gamma$ -ray background irregardless of whether the it is extragalactic, or contains a quasi-isotropic galactic or heliospheric emission component (Strong et al. 2004). Thus the number of background counts with energy  $E$  observed over the real time  $\Delta t = t_{wk}$  weeks is

$$B(> u) = \frac{X \Delta t E_{100} \pi \hat{\theta}^2 A_0 k_x}{2w + \alpha_B - 1 - a_0} u^{1+a_0-2w-\alpha_B}, \quad (\text{A8})$$

#### Source Counts

For a point source, the number of source counts with energy  $> E$  is given by

$$S(> E_1) \cong f_\gamma \int_0^{\Delta t} dt \int_{E_1}^{\infty} dE A[E, \theta(t), \phi(t)] \phi_s(E, t), \quad (\text{A9})$$

where  $\phi_s(E, t)$  is the source photon flux (ph cm<sup>-2</sup> s<sup>-1</sup> E<sup>-1</sup>) and we assume that the point spread function is defined as the  $f_\gamma = 68\%$  containment radius (see Thompson 1986). Thus

$$S(> u) \cong \frac{10^{-8} f_\gamma X_s \Delta t (\alpha_{ph} - 1) A_0 \phi_{-8}}{\alpha_{ph} - a_0 - 1} u^{1+a_0-\alpha_{ph}}, \quad (\text{A10})$$

and  $\alpha_{ph}$  is the photon number index (commonly denoted  $\Gamma$ ). The factor  $X_s$  accounts for the on-source exposure, and is generally equal to the background exposure factor  $X$ , though it may differ if one allows  $X_s$  to account for the source duty cycle, or if  $X$  accounts for variable background. The quantity  $\phi_{-8}$  normalizes the source flux

$$\phi_s(E) = \frac{10^{-8} (\alpha_{ph} - 1) \phi_{-8}}{E_{100}} u^{-\alpha_{ph}} \quad (\text{A11})$$

to 10<sup>-8</sup> ph( $E > 100$  MeV) cm<sup>-2</sup> s<sup>-1</sup>, which is the unit quoted by the EGRET team in the Third EGRET catalog (Hartman et al. 1999) for the two-week average fluxes.

For EGRET,  $S(> u) \cong 4.9 u^{-1.1} \phi_{-8} t_{wk} \geq 5 n_{5s}$ , where a source detection is assumed to require at least 5 counts ( $n_{5s} = 1$ ). From the signal limit, a minimum time

$$t_{wk}^E \gtrsim \frac{u^{\alpha_{ph}-1}}{\phi_{-8} X_s} n_5 \cong \frac{2u^{1.1}}{\phi_{-8}}, \quad (\text{A12})$$

is needed for EGRET to detect sources in the EGRET FOV as faint as  $\phi_{-8}$  (assuming that the blazar remains at the level of  $\phi_{-8}$  during the entire viewing period). Earth occultation means  $X_s \approx 1/2$ . The final expression in eq. (A12) applies when  $\alpha_{ph} = 2.1$ , the index of the isotropic  $\gamma$ -ray background. Here we suppose that blazars make a large fraction of the EGRB, and so must have a significant fraction of bright blazar sources emitting with  $\alpha_{ph} \cong 2.3$  between  $\approx 100$  MeV and 10 GeV.

For GLAST in the scanning mode, the condition for the detection of 5 counts is

$$t_{wk}^G \gtrsim \left( \frac{\alpha_{ph} - 1.16}{\alpha_{ph} - 1} \right) \frac{u^{\alpha_{ph}-1.16}}{X_{1/5} \phi_{-8}} n_{5s} \cong 0.85 \frac{u^{0.94}}{\phi_{-8}}, \quad (\text{A13})$$

where we have adopted a source occultation factor  $X_s = 0.2 X_{1/5}$ . The two estimates are similar at 100 MeV, because the factor 6 – 8 effective area advantage of GLAST over EGRET is reduced by GLAST in the scanning mode compared with the few occasions when the source is a pointing target for EGRET.

#### Signal to Background

From eqs. (A5), (A8) and (A10), the significance to detect a blazar at the  $n\sigma$  level is

$$n(> u) = \frac{S(> u)}{\sqrt{B(> u)}} = \frac{10^{-8} f_\gamma X_s \sqrt{A_0 \Delta t} \phi_{-8}}{\sqrt{X \pi k_x E_{100} \hat{\theta}}} \varphi_c u^{\varphi_x}, \quad (\text{A14})$$



where

$$\varphi_c = \frac{(\alpha_{ph} - 1)}{\alpha_{ph} - a_0 - 1} \sqrt{2w + \alpha_B - 1 - a_0}, \quad (\text{A15})$$

and

$$\varphi_x = w - \alpha_{ph} + \frac{1 + a_0 + \alpha_B}{2}. \quad (\text{A16})$$

The energy dependence of the background-limited detections of blazars is defined by the index

$$\varphi_x \cong \begin{cases} 2.05 - \alpha_{ph}, & \text{EGRET} \\ 2.30 - \alpha_{ph}, & \text{GLAST} \end{cases}, \quad (\text{A17})$$

and it is of interest that EGRET and GLAST are more sensitive to hard-spectrum blazars ( $\alpha_{ph} \lesssim 2 - 2.3$ ) at higher photon energies. This sensitivity improves until either there is a spectral break or softening, or the signal runs out.

The background limit on EGRET, with  $X = X_s$ , is

$$n^E(> u) = 0.36 \sqrt{X t_{wk} \phi_{-8}} u^{2.05 - \alpha_{ph}} > 5n_{5\sigma}. \quad (\text{A18})$$

Taking  $X = 0.5$ , due to Earth occultation, the number of weeks of direct pointing required for EGRET to detect a source with flux at the level  $\phi_{-8}$  at the  $5n_{5\sigma}$  significance level is

$$t_{wk}^E \gtrsim \frac{386}{\phi_{-8}^2} u^{2(\alpha_{ph} - 2.05)} n_{5\sigma}^2. \quad (\text{A19})$$

Comparison with eq. (A12) shows, as is well known, that signal detection with EGRET is background rather than signal limited. For  $u = 1$ , as used in the analysis reported in the EGRET catalogs, the limiting sensitivity to detect a strong source in a two-week pointing is

$$\phi_{-8} \gtrsim 14.$$

This estimate agrees well with detection data, as seen from Fig. 2.

For GLAST, the background limit translates into the condition

$$\phi_{-8} \gtrsim \frac{3.6n_{5\sigma}}{\sqrt{X t_{wk}}} u^{\alpha_{ph} - 2.3}, \quad (\text{A20})$$

so that the number of weeks of scanning required for GLAST to detect a source with flux level  $\phi_{-8}$  at the  $5n_{5\sigma}$  significance level is

$$t_{wk}^G \gtrsim \frac{64u^{2(\alpha_{ph} - 2.3)} n_{5\sigma}^2}{X_{1/5} \phi_{-8}^2} \rightarrow \frac{64}{\phi_{-8}^2} u^{-2/5}. \quad (\text{A21})$$

Thus, in around a year in the scanning mode, GLAST will detect sources at the level  $\phi_{-8} \sim 1$  when integrating above 100 MeV ( $u = 1$ ). This is not however the best detection strategy.

### *Optimal Source Detection with GLAST*

A better analysis considers optimal energy for source detection from both signal and noise limits. Equating eqs. (A13) and (A21) for the minimum time needed to detect sources at the  $5\sigma$ , 5 count limit assuming  $p = 3.2$  or  $\alpha_\nu = -0.1$ , gives the best lower photon energy above which to integrate, namely

$$\bar{u} \cong 20 \phi_{-8}^{-3/4}, \quad \text{or} \quad \bar{E} \cong 2.0 \phi_{-8}^{-3/4} \text{ GeV}. \quad (\text{A22})$$

The time it takes to reach this flux level is

$$\bar{t}_{wk} \cong \frac{14}{\phi_{-8}^{1.7}}. \quad (\text{A23})$$

Fig. 12 shows the minimum time for GLAST to detect sources at different integral flux levels  $\phi_{-8}$  and with different spectral indices from the signal and background limits, eqs. (A13) and (A21), respectively. In order to determine the source's spectral index, a hardness ratio or mean photon energy  $\langle E \rangle$  can be calculated for photons originating from a source at a known source position. For photons with energies between 100 MeV and  $E_2 = 100u_2$  MeV originating from a source with spectral index  $\alpha_{ph}$ ,

$$\langle E \rangle = E_{100} \left( \frac{\alpha_{ph} - 1 - a_0}{\alpha_{ph} - 2 - a_0} \right) \frac{1 - u_2^{\alpha_{ph} - 2 - a_0}}{1 - u_2^{\alpha_{ph} - 1 - a_0}}. \quad (\text{A24})$$

Background contamination must also be considered to determine the best value and error for  $\alpha_{ph}$ . The upper energy used for  $u_2$  depends on the nature of the source spectrum or the cutoff produced by  $\gamma\gamma$  attenuation on the EBL. For low redshift sources, contemporaneous observations with MAGIC, HESS, or VERITAS ground-based  $\gamma$ -ray telescopes could

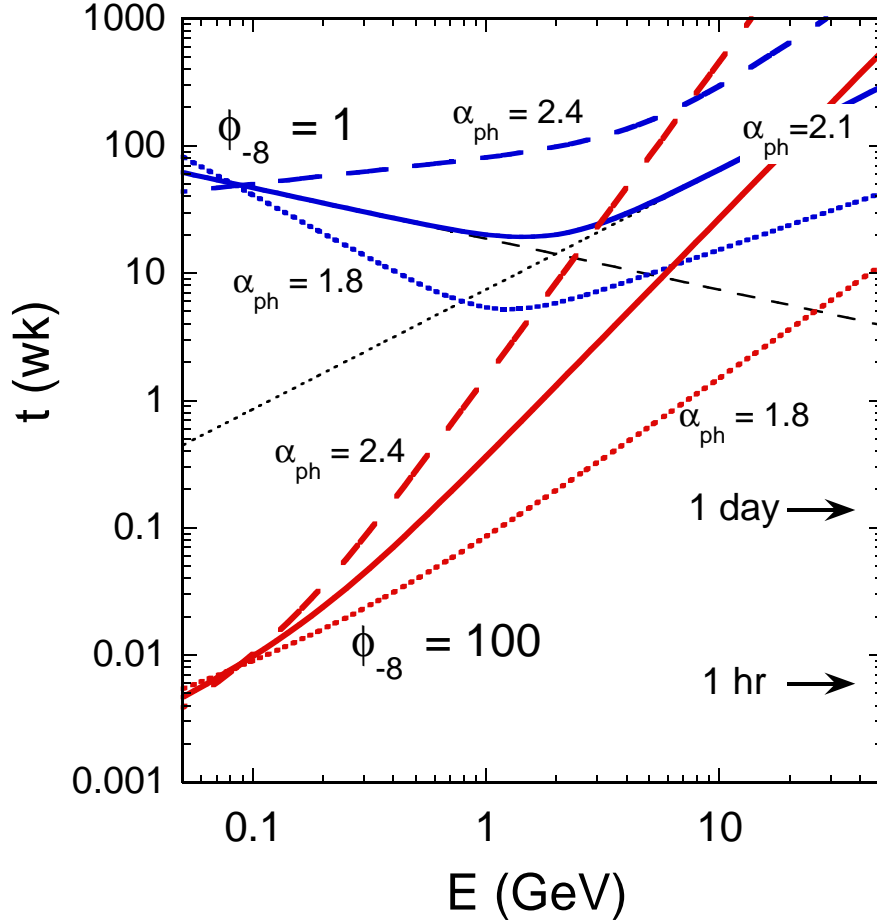


FIG. 9.— Time required for GLAST in the scanning mode to detect a source at integral flux levels  $\phi_{-8} = 1$  and  $\phi_{-8} = 100$  when integrating signal above energy  $E$ , for sources with photon spectral indices  $\alpha_{ph} = 2.4$  (thick long-dashed curves),  $\alpha_{ph} = 2.1$  (thick solid curves), and  $\alpha_{ph} = 1.8$  (thick dotted curves). Light dotted and dashed lines show the time required to detect a source from signal and background limits, respectively, for  $\phi_{-8} = 1$  and  $\alpha_{ph} = 2.1$ .

help constrain the upper energy. Higher energy analysis can enhance blazar detection. For example, Dingus & Bertsch (2001) reported the search for blazars in the EGRET data by looking at  $> 10$  GeV photons.

From the previous considerations and from Fig. 9, weak sources are best identified with GLAST by calculating the statistical significance  $S(> E)/\sqrt{B(> E)}$  of a source as a function of photon energy  $E$ , and searching for the minimum in the detection significance. The actual measurement consists of the sum  $S(> E)$  and  $B(> E)$ , and the value of  $B(> E)$  is calculated from our knowledge of the diffuse galactic and extragalactic background and GLAST detection characteristics. Knowledge of  $B(> E)$  will improve with our understanding of the GLAST results. For sources with spectra harder than the diffuse EGRB, a minimum in the combined background and signal-limited significance will be found by this procedure. This represents a systematic bias for GLAST to discover hard spectrum sources, and must also be considered when treating population statistics. At the same time, an unbiased search for sources with fluxes above a fixed energy  $E$ , e.g.,  $E = 100$  MeV, 1 GeV, and 10 GeV should also be made with GLAST.

#### Short Timescale Flares

GLAST reaches EGRET 2-week sensitivities of  $\phi_{-8} \cong 15$  after  $\approx 1 - 2$  days, as can be obtained by comparing eq. (A23) with eq. (A21). It reaches this sensitivity over the *full sky*, compared to  $\approx 1/24^{th}$  of the full sky viewed with EGRET. For a mean photon energy of  $\approx 400$  MeV measured with EGRET from a blazar with  $2 \lesssim \alpha_{ph} \lesssim 2.5$ , a measurement of  $\phi_{-8} \cong 15$  (150) corresponds to an energy flux between 100 MeV and 5 GeV of  $\cong 10^{-10}$  ( $10^{-9}$ ) ergs  $\text{cm}^{-2} \text{s}^{-1}$ .

Consider a flare at the level of  $\phi_{-8} \cong 200$ , corresponding to some of the brightest flares seen with EGRET. Given the Phase 1 EGRET all-sky survey results (Dermer & Dingus 2003), we predict a flare at this level every few days, with large uncertainties given the small statistics of bright blazar flares. For a blazar with  $\gamma$ -ray spectral index  $\alpha_{ph} = 2.1$ , GLAST will have a significant  $5\sigma$  detection after

$$\bar{t} \cong 2.6 \text{ ks} , \quad (\text{A25})$$

using  $\bar{u} = 1$  whenever  $\bar{u} < 1$ . Better sensitivity of a bright blazar flare is possible for observing times less than the GLAST orbital period of 1.6 hr (or 5.8 ks) if the blazar is in the FOV of GLAST. In this case,  $X_s$  can be larger

than 1/5. These timescales are of particular interest inasmuch as we expect a minimum variability timescale  $t_{var}$  corresponding to a light-crossing distance

$$t_{var} = \frac{2GM}{c^3} (1+z) \approx M_8(1+z) \text{ ks}; \quad (\text{A26})$$

corrections should be made to this expression for a Kerr metric. Temporal power analyses of strings of data from bright blazars, such as 3C 279 and PKS 0528+134, could find a reduction of power at a timescale corresponding to the Schwarzschild radius or radius of the minimum stable orbit. Rare, bright, hard spectrum flares are of particular interest for GLAST analysis in order to look for  $\gamma\gamma$  absorption cutoffs, whether internal (within the blob), external within the inner jet or galactic environment, or due to absorption on diffuse radiation fields.

#### SYNCHROTRON SELF-ABSORPTION FREQUENCY

We calculate the synchrotron self-absorption (SSA) frequency in terms of the parameters of the system,  $l'_e, \Gamma$ , and  $z$ . Using the formalism of Gould (1979), cast into dimensionless notation, we have the expression for the frequency  $\nu_m$  where  $dF_\nu(\nu_m)/d\nu = 0$ , given by

$$\epsilon_m = \frac{h\nu_m}{m_e c^2} = \frac{\delta_D}{1+z} \left[ \frac{4\pi c(p)}{\alpha_f t_m} r'_b r'_e k'_e \right]^{2/(p+4)} b^{(p+2)/(p+4)}, \quad (\text{B1})$$

and  $c(p)$  and  $t_m$  are numbers of order unity (Gould 1979),  $\alpha_f = 1/137$  is the fine structure constant, and  $K'_e = V'_b k'_e$ . From the expression for synchrotron radiation, eq. (10),

$$l'_e = \left( \frac{2c\sigma_T U_{B_{cr}}}{9} \right) k'_e r'_b{}^3 b^{(p+1)/2}. \quad (\text{B2})$$

It follows from these expressions

$$\epsilon_m = \frac{\nu(\text{GHz})}{1.2 \times 10^{11}} = \frac{\delta_D}{1+z} \left[ \frac{18\pi c(p)}{\alpha_f t_m} \frac{l'_e}{c\sigma_T U_{B_{cr}}} \left( \frac{r_e}{r'_b} \right)^2 \right]^{3/(p+4)} b^{1/(p+4)}. \quad (\text{B3})$$

We obtain

$$\nu(\text{GHz}) \cong \frac{\delta_D}{1+z} \begin{cases} 0.22 (\sqrt{l_{42}/r_{14}}) B(\text{G})^{1/6}, & p = 2 \\ 9.5 (l_{42}/r_{14}^2)^{3/7} B(\text{G})^{1/7}, & p = 3 \\ 1900 (l_{42}/r_{14}^2)^{3/8} B(\text{G})^{1/8}, & p = 4 \end{cases} \quad (\text{B4})$$

where  $r'_b = 10^{14} r_{14}$  cm and  $l'_e = 10^{42} l_{42}$  ergs s<sup>-1</sup> sr<sup>-1</sup>. BLs are likely to be heavily self-absorbed at 5 GHz, using parameters  $\delta_D \cong 4$ ,  $p = 3$ ,  $l_{42} \cong 1$ ,  $r_{14} \cong 1$ , and  $B \cong 0.1 - 1$  G. FSRQs could also be self-absorbed at 5 GHz, using  $\delta_D \cong 10$ ,  $p > 3$ ,  $l_{42} \cong 0.01$ ,  $r_{14} \cong 100$ , and  $B \gtrsim 1$  G. Here the values of  $B$  are typical of equipartition magnetic field strengths. If GLAST shows that FSRQs vary on hour or sub-hour timescales, then the synchrotron emission of blazars is likely to be strongly self-absorbed.

#### REFERENCES

- Bade, N., Beckmann, V., Douglas, N. G., Barthel, P. D., Engels, D., Cordis, L., Nass, P., & Voges, W. 1998, *A&A*, 334, 459  
Blain, A. W., Jameson, A., Smail, I., Longair, M. S., Kneib, J.-P., & Ivison, R. J. 1999, *MNRAS*, 309, 715  
Błażejowski, M., Sikora, M., Moderski, R., & Madejski, G. M. 2000, *ApJ*, 545, 107  
Böttcher, M., & Dermer, C. D. 2002, *ApJ*, 564, 86  
Cavaliere, A., & D'Elia, V. 2002, *ApJ*, 571, 226  
Chiang, J., Fichtel, C. E., von Montigny, C., Nolan, P. L., & Petrosian, V. 1995, *ApJ*, 452, 156; (e) 1996, *ApJ*, 465, 1011  
Chiang, J., and Mukherjee, R. 1998, *ApJ*, 496, 752  
Dermer, C. D. 2006, in Proc. of "The Multi-Messenger Approach to High-Energy Gamma-ray Sources," Barcelona, Spain (astro-ph/0610195)  
Dermer, C. D., & Dingus, B. L. 2003, *New Astronomy Rev.*, 48, 537  
Dermer, C. D., & Schlickeiser, R. 2002, *ApJ*, 575, 667  
Dermer, C. D., & Davis, S. P. 2000, in the Fifth Compton Symposium (AIP: New York), ed. M. L. McConnell & J. M. Ryan, 510, 425  
Dermer, C. D., Sturmer, S. J., & Schlickeiser, R. 1997, *ApJS*, 109, 103  
Dermer, C. D., and Gehrels, N. 1995, *ApJ*, 447, 103; (e) 1996, *ApJ*, 456, 412  
Dermer, C. D. 1995, *ApJ*, 446, L63  
Dermer, C. D. 1992, *Phys. Rev. Lett.*, 68, 1799  
Dingus, B. L., & Bertsch, D. L. 2001, *AIP Conf. Proc.* 587: Gamma 2001: Gamma-Ray Astrophysics, 587, 251  
Fichtel, C. E., et al. 1994, *ApJS*, 94, 551  
Fossati, G., Maraschi, L., Celotti, A., Comastri, A., & Ghisellini, G. 1998, *MNRAS*, 299, 433  
Georganopoulos, M., Kirk, J. G., & Mastichiadis, A. 2001, *ApJ*, 604, 479; (e) 2001, *ApJ*, 561, 111  
Georganopoulos, M., & Kazanas, D. 2003, *ApJ*, 594, L27  
Ghisellini, G., Tavecchio, F., & Chiaberge, M. 2005, *A&A*, 432, 401  
Ghisellini, G., & Celotti, A. 2001, *A&A*, 379, L1  
Ghisellini, G., Celotti, A., Fossati, G., Maraschi, L., & Comastri, A. 1998, *MNRAS*, 301, 451  
Giommi, P., Menna, M. T., & Padovani, P. 1999, *MNRAS*, 310, 465  
Giommi, P., Pellizzoni, A., Perri, M., & Padovani, P. 2001, *ASP Conf. Ser.* 227: Blazar Demographics and Physics, 227, 227  
Giommi, P., Colafrancesco, S., Cavazzuti, E., Perri, M., & Pittori, C. 2006, *A&A*, 445, 843  
Gould, R. J. 1979, *A&A*, 76, 306  
Haiman, Z., Ciotti, L., & Ostriker, J. P. 2004, *ApJ*, 606, 763  
Hartman, R. C. et al. 1999, *ApJS*, 123, 79  
Hopkins, A. W., & Beacom, J. F. 2006, *ApJ*, 651, 142

- Huang, J.-S., Glazebrook, K., Cowie, L. L., & Tinney, C. 2003, *ApJ*, 584, 203
- Jorstad, S. G., Marscher, A. P., Mattox, J. R., Wehrle, A. E., Bloom, S. D., & Yurchenko, A. V. 2001, *ApJS*, 134, 181
- Jorstad, S. G., Marscher, A. P., Mattox, J. R., Aller, M. F., Aller, H. D., Wehrle, A. E., & Bloom, S. D. 2001a, *ApJ*, 556, 738
- Kataoka, J., et al. 1999, *ApJ*, 514, 138
- Krawczynski, H., et al. 2001, *ApJ*, 559, 187
- Kühr, H., Witzel, A., Pauliny-Toth, I. I. K., & Nauber, U. 1981, *A&AS*, 45, 367
- Le, T., & Dermer, C. D. 2006, *ApJ*, submitted (astro-ph/0610043)
- Li, P.-P., & Ma, Y.-Q. 1983, *ApJ*, 272, 317
- Lind, K. R., & Blandford, R. D. 1985, *ApJ*, 295, 358
- Maraschi, L., Ghisellini, G., & Celotti, A. 1992, *ApJ*, 397, L5
- Maraschi, L., & Tavecchio, F. 2003, *ApJ*, 593, 667
- Mücke, A., & Pohl, M. 2000, *MNRAS*, 312, 177
- Mücke, A., et al. 1997, *A&A*, 320, 33
- Mukherjee, R., et al. 1996, *ApJ*, 470, 831
- Mukherjee, R., et al. 1997, *ApJ*, 490, 116
- Narumoto, T., & Totani, T. 2006, *ApJ*, 643, 81
- Padovani, P. and Giommi, P. 1995, *MNRAS*, 277, 1477
- Padovani, P. and Giommi, P. 1995a, *ApJ*, 444, 567
- Perlman, E. S., et al. 1996, *ApJS*, 104, 251
- Petry, D., et al. 2000, *ApJ*, 536, 742
- Rector, T. A., Stocke, J. T., Perlman, E. S., Morris, S. L., & Gioia, I. M. 2000, *AJ*, 120, 1626
- Romani, R. W., Sowards-Emmerd, D., Greenhill, L., & Michelson, P. 2004, *ApJ*, 610, L9
- Sambruna, R. M., Maraschi, L., & Urry, C. M. 1996, *ApJ*, 463, 444
- Sanders, D. B., & Mirabel, I. F. 1996, *ARA&A*, 34, 749
- Sanders, D. B. 2004, *Advances in Space Research*, 34, 535
- Sikora, M., Madejski, G., Moderski, R., & Poutanen, J. 1997, *ApJ*, 484, 108
- Sowards-Emmerd, D., Romani, R. W., Michelson, P. F., Healey, S. E., & Nolan, P. L. 2005, *ApJ*, 626, 95
- Spiegel, D. N., et al. 2003, *ApJS*, 148, 175
- Sreekumar, P., et al. 1998, *ApJ*, 494, 523
- Stawarz, L., Kneiske, T. M., & Kataoka, J. 2006, *ApJ*, 637, 693
- Stecker, F. W., & Salamon, M. H. 1996, *ApJ*, 464, 600
- Strong, A. W., Moskalenko, I. V., & Reimer, O. 2000, *ApJ*, 537, 763; (e) 2000, *ApJ*, 541, 1109
- Strong, A. W., Moskalenko, I. V., & Reimer, O. 2004, *ApJ*, 613, 956
- Thompson, D. J., 1986, *Nuclear Instruments and Methods in Physics Research*, A251, 390
- Urry, C. M., and Padovani, P. 1995, *PASP*, 107, 803
- Vermeulen, R. C., & Cohen, M. H. 1994, *ApJ*, 430, 467

TABLE 1  
SAMPLE OF HIGH-CONFIDENCE GAMMA-RAY BLAZARS USED IN ANALYSIS

Catalog Name	$\phi_{-8}^{pk}$ <sup>a</sup>	$\Delta\phi_{-8}^{pk}$	Redshift $z$	Other Name <sup>b</sup>	Classification <sup>c</sup>
3EG J0204+1458	52.8	26.4	0.405	PKS 0202+14	
3EG J0210-5055	134.1	24.9	1.003	PKS 0208-512	
3EG J0222+4253	25.3	5.80	0.444	3C 66A	B
3EG J0237+1635	65.1	8.80	0.940	AO 0235+164	B
3EG J0340-0201	177.6	36.6	0.852	PKS 0336-01	
3EG J0412-1853	49.5	16.1	1.536	PKS 0414-189	
3EG J0422-0102	64.2	34.2	0.915	PKS 0420-01	
3EG J0442-0033	85.9	12.0	0.844	NRAO 190	
3EG J0450+1105	109.5	19.4	1.207	PKS 0446+112	
3EG J0456-2338	14.7	4.20	1.009	PKS 0454-234	
3EG J0458-4635	22.8	7.40	0.8580	PKS 0454-46	
3EG J0459+0544	34.0	18.0	1.106	PKS 0459+060	
3EG J0500-0159	68.2	41.3	2.286	PKS 0458-02	
3EG J0530+1323	351.4	36.8	2.060	PKS 0528+134	
3EG J0540-4402	91.1	14.6	0.894	PKS 0537-441	B
3EG J0721+7120	45.7	11.1	0.30	S5 0716+714	B
3EG J0737+1721	29.3	9.90	0.424	PKS 0735+178	B
3EG J0743+5447	42.1	8.30	0.723	RX J0742.6+5444	
3EG J0828+0508	35.5	16.3	0.180	PKS 0829+046	B
3EG J0829+2413	111.0	60.1	0.939	OJ 248	
3EG J0845+7049	33.4	9.00	2.172	4C 71.07	
3EG J0852-1216	44.4	11.6	0.566	PMN J0850-1213	
3EG J0853+1941	15.8	6.90	0.306	OJ 287	B
3EG J0952+5501	47.2	15.5	0.901	OK 591	
3EG J0958+6533	18.0	9.40	0.368	S4 0954+65	B
3EG J1104+3809	27.1	6.90	0.031	Mkn 421	B
3EG J1200+2847	163.2	40.7	0.729	TON 0599	
3EG J1222+2841	53.6	14.1	0.102	W Comae	B
3EG J1224+2118	48.1	15.3	0.435	PG 1222+216	
3EG J1229+0210	48.3	11.3	0.158	3C 273	
3EG J1230-0247	15.5	4.10	1.045	PKS 1229-02	
3EG J1246-0651	44.1	29.6	1.286	PKS 1243-072	
3EG J1255-0549	267.3	10.7	0.538	3C 279	
3EG J1329+1708	33.1	19.3	2.084	OP 151	
3EG J1339-1419	20.2	11.6	0.539	PKS 1335-127	
3EG J1409-0745	128.4	23.4	1.494	PKS 1406-076	
3EG J1429-4217	55.3	16.3	1.522	PKS 1424-41	
3EG J1512-0849	49.4	18.3	0.361	PKS 1510-08	
3EG J1605+1553	42.0	12.3	0.357	4C 15.54	B
3EG J1608+1055	62.4	13.0	1.226	OS 111	
3EG J1614+3424	68.9	15.3	1.401	OS 319	
3EG J1625-2955	258.9	15.3	0.815	PKS 1622-29	
3EG J1626-2519	82.5	35.0	0.786	PKS 1622-253	
3EG J1635+3813	107.5	9.60	1.814	4C 38.41	
3EG J1727+0429	30.2	18.8	0.296	PKS 1725+044	
3EG J1733-1313	104.8	34.7	0.902	PKS 1730-13	
3EG J1738+5203	44.9	26.9	1.375	OT 566	
3EG J1744-0310	48.7	19.6	1.054	PKS 1741-03	
3EG J1935-4022	93.9	31.4	0.966	PKS 1933-400	
3EG J1937-1529	55.0	18.6	1.657	PKS 1936-15	
3EG J2025-0744	74.5	13.4	1.388	PKS 2023-07	
3EG J2036+1132	35.9	15.0	0.601	TXS 2032+117	B
3EG J2055-4716	35.0	20.9	1.489	PKS 2052-47	
3EG J2158-3023	30.4	7.70	0.116	PKS 2155-304	B
3EG J2202+4217	39.9	11.6	0.069	BL Lac	B
3EG J2232+1147	51.6	15.0	1.037	CTA 102	
3EG J2254+1601	116.1	18.4	0.859	3C 454.3	
3EG J2321-0328	38.2	10.1	1.411	PKS 2320-035	
3EG J2358+4604	42.8	20.3	1.992	OZ 486	
3EG J2359+2041	26.3	9.00	1.066	OZ 193	

<sup>a</sup>  $\phi_{-8}^{pk}$ : peak flux ( $E > 100$  MeV) in units of  $10^{-8}$  photons  $\text{cm}^{-2}$   $\text{s}^{-1}$ .

<sup>b</sup> Survey catalogs include PKS: Parkes, O(A-Z): Ohio, 3C/4C: Cambridge, and TXS: Texas.

<sup>c</sup> B: BL Lac object; no entry: FSRQ.